https://doi.org/10.5194/egusphere-2024-1509
Preprint. Discussion started: 22 October 2024

Development and assessment of the physical-biogeochemical ocean regional model in the Northwest Pacific: NPRT v1.0 (ROMS v3.9–TOPAZ v2.0)

Daehyuk Kim[1], Hyun-Chae Jung[4], Jae-Hong Moon[1,2,3], Na-Hyeon Lee[3]

[1] *Center for Sea Level Changes, Jeju National University, Jeju, 63243, Republic of Korea*

[2] *Department of Earth and Marine Sciences, Jeju National University, Jeju, 63243, Republic of Korea*

[3] *Faculty of Earth and Marine Convergence, Earth and Marine Science Major, Jeju National University, Jeju, 63243, Republic of Korea*

[4] *Department of Earth and Environmental Sciences, Jeonbuk National University, Jeonju, 54896, Republic of Korea*

Corresponding author: Jae-Hong Moon, jhmoon@jejunu.ac.kr

https://doi.org/10.5194/egusphere-2024-1509
Preprint. Discussion started: 22 October 2024

Abstract

The biogeochemical cycling system exhibits diverse characteristics in different regions owing to various factors. The Northwest Pacific is characterized by the presence of the warm and nutrient-depleted Kuroshio Current and the cold and nutrient-enriched Oyashio Current. In this region, surface primary production leads to increased nutrient consumption and CO_2 exchange. The Yellow and East China Seas (YECS) are predominantly influenced by freshwater input. A high resolution regional numerical model tailored to the specific features of each area is required to reproduce the different characteristics of each region. Therefore, to accurately analyze the physical and biogeochemical system, this study developed a new coupled physical-biogeochemical model combining the three-dimensional Regional Ocean Modeling System (ROMS) and the Generic Ocean Turbulence Model Tracers of Phytoplankton with Allometric Zooplankton (TOPAZ) for the Northwest Pacific, including the YECS. The simulated physical and biogeochemical variables in the ROMS–TOPAZ (NPRT) were evaluated by comparing them with available observational data. The spatial correlation ranges of the various variables reproduced in the NPRT were 0.5–0.7. In the upper layer (0–20 m), NPRT successfully simulated the seasonal variability of chlorophyll, capturing two peaks in spring and summer, which were not captured by the CMIP6 data. Particularly in the YECS, NPRT effectively represented the biomass driven by riverine effect, which is difficult to reproduce in global biogeochemical model with low-resolution. However, NPRT still exhibits significant biases in the subarctic region and marginal seas. To minimize the uncertainties in biogeochemical variables, it is necessary to refine the initial and boundary conditions, adjust parameters, and apply discharge forcing based on observational data. Despite these limitations, NPRT is an important tool for studying the interaction between ocean physics and biogeochemistry at a high resolution.

1. Introduction

The pronounced global climate change tends in the 21st century have increased interest in various research fields, including physical oceanography, atmospheric science, and biogeochemistry. The recent exponential increase in computer resources has enabled us to consider simultaneously two or more disciplines and conduct numerical studies on complex interactions among various fields. The ocean biogeochemical processes are among the most important fields for understanding Earth's carbon and ecosystem cycles, as well as the global climate system (Reid et al., 2009; Kang et al., 2017; Park et al., 2014, 2018, Lee et al., 2022). Previous studies utilized Earth system models to analyze ocean biogeochemistry, climate feedback, and the carbon cycle (Kang et al., 2017; Park et al., 2018; 2019). In particular, significant efforts have been made to analyze physical–biogeochemical features at the global

https://doi.org/10.5194/egusphere-2024-1509
Preprint. Discussion started: 22 October 2024

scale as well as at regional scales (Hauri et al., 2020; Zhao et al., 2021; Wu et al., 2023; Na et al., 2024).

The North Pacific is a key region where the biological carbon pump occurs effectively (Chierici et al., 2006; Takahashi et al., 2009). Low-frequency physical and ecological variabilities in the North Pacific are closely related to various climatological variability patterns, such as the Pacific Decadal Oscillation (PDO) and El Niño–Southern Oscillation (ENSO). Numerous studies have been conducted on the responses of ecosystems to climatic and environmental conditions influenced by these long-term climatological variability patterns, especially in the Northeast Pacific (Overland et al., 2008; Yatsu et al., 2013; Ma et al., 2020). However, in the Northwest Pacific including marginal seas, regional-scale oceanographic and ecological variabilities are more important than climatological variability patterns, i.e., PDO and ENSO (Jung et al., 2017; Ma et al., 2020). In particular, the Northwest Pacific is known as the Kuroshio–Oyashio Confluence Region (Kawai, 1972; Hanawa and Mitsudera, 1987); the Oyashio Current is formed from the East Kamchatka Current, flowing southwestward along the Hokkaido coast while mixing with the Okhotsk Sea Mode Water, and the Kuroshio Current flows northeastward along the east of Japan, originating from Luzon Island (Nitani, 1972). Therefore, this region is known for the convergence of distinct water properties, resulting in a complex frontal structure, thermohaline mixing, and significant variability in the upper layer circulation (Qiu, 2001; Yasuda, 2003; Taguchi et al., 2007). Specifically, the water mass of the Oyashio Current has low temperature and low salinity, i.e., lower than 7 °C and 33.7 psu at a depth of 100 m (Kawai, 1972). Conversely, the water mass of the Kuroshio Current has a temperature higher than 14 °C and salinity higher than 34.7 psu (Nitani, 1972; Wang et al., 2022). In this region, the biogeochemical characteristics also exhibit significant regional differences. The cyclonic subarctic gyre, located west of the Oyashio Current, is characterized by high nutrient levels and low chlorophyll concentration (Taniguchi, 1999). Conversely, the anticyclonic tropical gyre, situated in the Kuroshio Current, is characterized by low nutrient levels (Siswanto et al., 2015). The interaction between these gyres with distinct biogeochemical characteristics results in increased nutrient availability and the simulation of high biomass (Shiozaki et al., 2014). Consequently, the Northwest Pacific has been extensively studied from the perspectives of hydrography, climate change, nutrient transport, the carbon cycle, phytoplankton production, and community structure in relation to external conditions (Okamoto et al., 2010; Kuroda et al., 2019; Wang et al., 2021).

The Northwest Pacific is an important region for understanding the global carbon cycle and enhancing its predictability. Many previous studies have analyzed the carbon cycle, ecosystems, and future climate change using low-resolution global climate models with biogeochemical modules (Park et al., 2014; Jung et al., 2019; Hauri et al., 2020; Lee et al., 2022). However, coupled physical–biogeochemical ocean models with low horizontal resolutions involve limitations regarding accurately reproducing and analyzing the characteristics of oceanic environmental systems particularly the

https://doi.org/10.5194/egusphere-2024-1509
Preprint. Discussion started: 22 October 2024

physical–biogeochemical factors in regional areas. Therefore, in this study, to accurately understand the physical–biogeochemical processes at the regional scale and address uncertainties, a regional ocean model and a biogeochemical model were coupled at a high resolution. Specifically, we employed the Generic Ocean Turbulence Model–Tracers of Phytoplankton with Allometric Zooplankton (TOPAZ) developed by the US National Oceanic and Atmospheric Administration's Geophysical Fluid Dynamics Laboratory (GFDL), in conjunction with the Regional Ocean Modeling System (ROMS).

This study introduces a new high-resolution coupled physical-biogeochemical model, named the "Northwest Pacific ROMS–TOPAZ model version 1.0 (hereafter NPRT)", which is a valuable tool for not only understanding the interactions between physical and biogeochemical processes but also for predicting the future ocean carbon system. We describe and evaluate the simulation results of the coupled physical–biogeochemical model (NPRT) through comparison with available observational data. Sections 2.1 and 2.2 describe the characteristics of the models used in this study, and Section 2.3 and 2.4 elaborate on the developed NPRT, the methodology behind it, and the specific model design for the study area. In section 3, the model results are evaluated using observations of physical and biogeochemical variables, such as sea surface height (SSH), salinity, chlorophyll, nutrients, dissolved inorganic carbon (DIC), and dissolved oxygen (DO). In addition, we analyze the characteristics of the physical–biogeochemistry regional ocean model with high resolution. Finally, a summary and discussion are presented in section 4.

2. Data and model

2.1 Physical Ocean model (ROMS v3.9)

For conducting the physical–biogeochemical model coupling in this study, we employed ROMS version 3.9 (hereafter ROMS; Song and Haidvogel, 1994), which is a popular physical regional ocean model. ROMS is a three-dimensional primitive-equation physical ocean model that uses hydrostatic and Boussinesq approximations. The horizontal grid system is the Arakawa-C grid system, which enhances computational stability and efficiency (Arakawa and Lamb, 1977). The vertical coordinate system is the S-coordinate (stretched terrain-following coordinate), which combines the advantages of implementing the z-coordinate for the planetary boundary layer (PBL) and the σ-coordinate for the bottom boundary layer. In this way, it allows for accurate analyses of physical phenomena in the thermocline or bottom boundary layer, while reducing pressure gradient errors that are sensitive to the terrain (Song and Wright, 1998; Shchepetkin and McWilliams, 2003).

ROMS can utilize horizontal advection schemes, such as second-, and fourth-order centered

https://doi.org/10.5194/egusphere-2024-1509
Preprint. Discussion started: 22 October 2024

differences and a third-order upstream scheme. Various options are available for vertical mixing, including the K-profile parameterization (KPP; Large et al., 1994), M–Y (Mellor and Yamada, 1982), Generic Length Scale (GLS; Umlauf and Burchard, 2003). In addition, bulk parameterization involving the wind, sensible heat flux, and latent heat flux provides better calculations of the heat budget changes, which is essential for elucidating the atmosphere–ocean interactions (Fairall et al., 1996). For more information on ROMS, we refer to Shchepetkin and McWilliams (2005) and McWilliams (2009).

2.2 Biogeochemical model (TOPAZ v2.0)

TOPAZ version 2.0 (hereafter TOPAZ) is a biogeochemical module that simulates the cycles of carbon, nitrogen, phosphorus, silicon, iron, DO, and lithogenic material, while also considering the growth cycles of the zooplankton and phytoplankton. In biogeochemical processes, phytoplankton members are categorized based on their sizes into small and large, including the nitrogen-fixing diazotrophs. Overall, TOPAZ handles a total of 30 prognostic and 11 diagnostic tracers, and the state variable *C* in various tracers reproduced in TOPAZ can be calculated using the following continuity equation to describe local changes.

$$\frac{\partial C}{\partial t} = -\nabla \cdot \tilde{v}C + \nabla K \nabla C + S_c, \qquad (1)$$

where $\tilde{v}$ and K represent the vector velocity and diffusivity, respectively, and S_c indicates the source-minus-sink terms of the state variable *C* calculated at each grid. TOPAZ considers eight types of biogeochemical processes: the dissolved organic matter (DOM) cycle, particle sinking, dry/wet atmospheric decomposition, gas exchange, river input, removal, sediment input and scavenging (Dunne et al., 2005; 2007). Various equations for these processes are available, utilizing relationships between variables derived from observational data (Dunne et al., 2012). In addition, TOPAZ includes an "optical feedback" module that considers the chlorophyll photosynthesis. Optical feedback calculates the total surface irradiance(*I(z)*) as a function of the solar radiation wavelength (Manizza et al., 2005). This scheme regulates vertically penetrating irradiance due to shortwave radiation absorption in the visible light, which is influenced by the distribution of chlorophyll concentration in the water column of the model.

$$I(z) = I_{IR} \cdot e^{-k_{IR}^{2}} + I_{RED(z-1)} \cdot e^{-k_{(r)}\Delta z} + I_{BLUE(z-1)} \cdot e^{-k_{(b)}\Delta z}, \qquad (2)$$

where the first term in the right hand side represents the penetration of the infrared wavelength band, and the second and third terms represent the photosynthetically active radiation (PAR), which is divided into two visible wavelength bands, namely the red and blue/green bands. PAR is used to calculate the

https://doi.org/10.5194/egusphere-2024-1509
Preprint. Discussion started: 22 October 2024

growth rate of phytoplankton groups and is a key factor in biogeochemistry. For more detailed information on TOPAZ, we refer to Dunne et al. (2012).

2.3 The coupled ROMS–TOPAZ model (NPRT version 1.0)

In this study, to couple ROMS with TOPAZ, we employed the stand-alone version of TOPAZ, which was separated from the Modular Ocean Model version 5 (MOM5) developed by the GFDL in a previous study (Jung et al., 2019). In this study for the stand-alone version of TOPAZ, the air–sea gas exchange for CO_2 and O_2 is based on Wanninkhof (1992) and Najjar and Orr (1998), and the optical feedback is based on Manniza et al. (2005). Furthermore, TOPAZ prescribes the surface flux from the atmosphere to the ocean for DIC, DO, nitrate (NO_3), ammonia (NH_4), alkalinity (Alk), lithogenic aluminosilicate (LITH), dissolved iron (Fed), and phosphate (PO_4) (Jung et al., 2019). For these atmospheric chemistry values for the surface flux, this study employs climatological data with seasonal variations.

Fig. 1 shows the structure of the NPRT. During the initialization process, TOPAZ receives the grid and domain information from ROMS. Subsequently, integration with the *ROMS Main Driver* occurs to calculate S_c within the "time step loop" using Eq. (1). Simultaneously, the chlorophyll optical feedback is also considered in each time step, with the PAR modified by chlorophyll concentrations influencing S_c, whereas the total radiation is used in the physical processes of ROMS. In the *ROMS Main Driver*, the advection and diffusivity terms are calculated considering river runoff (Alk, DIC, NH_4, NO_3, LITH, and PO_4). Information such as prognostic tracers, ocean physical variables, atmospheric forcing, and dry/wet deposition (Alk, LITH, NH_4, NO_3, and Fed) are then transmitted to the TOPAZ module, where the source/sink term (S_c) is calculated. In other words, the state variable C is calculated using data related to the transport tendency of the tracers and source/sink term through the *ROMS physics* and *generic_TOPAZ_column_physics* modules (Fig. 1).

2.4 Experimental setup

To operate NPRT, it is necessary to obtain the initial and boundary conditions for the biogeochemical variables considered by TOPAZ; however, it is impossible to encompass all biogeochemical observational data, since TOPAZ considers 30 prognostic and 11 diagnostic tracers. Therefore, in this study, the results of MOM–TOPAZ were employed as the initial and boundary conditions of TOPAZ. To operate MOM5–TOPAZ, the default input datasets provided by the official MOM GitHub (https://mom-ocean.github.io/docs/quick-start-guide/, last access: 1 March 2023) were employed for the initial condition. MOM–TOPAZ was initially operated for a 100-year spin-up integration under a pCO_2 environment (369.6 ppm) and ECMWF Reanalysis v5 (ERA5; Hersbach et al. 2020) of year 2000. Séférian et al. (2016) suggested that biochemical models require spin-up times

https://doi.org/10.5194/egusphere-2024-1509
Preprint. Discussion started: 22 October 2024

longer than those required by physical ocean models. However, in this study, we adopted a 100-year spin-up time integration because of limited computing and time resources. After the 100-year spin-up time integration, using the results from the last time step as the initial condition, MOM5–TOPAZ was operated for 2000–2014, with a realistic atmospheric CO_2 concentration and atmospheric forcings from ERA5. Through these spin-up process described above, the initial and boundary conditions for the biogeochemical variables required to conduct NPRT were obtained. Nutrient concentrations for dry/wet atmospheric deposition and runoff were obtained from the default input data of the official MOM GitHub.

The initial and boundary conditions used for the physical variables were monthly mean data from the Hybrid Coordinate Ocean Model (HYCOM) reanalysis with a 1/12° horizontal resolution. We used the six-hourly atmospheric external forcings, as provided by ERA5 as well as climatological monthly mean discharges of 12 major rivers, including the Yangtze, Huanghe, Yungsan, Keum, Han, Haihe, Luanhe, Amnokgang, Taedong, Qiantang, Pearl Rivers (Fig. 2; Kwon 2007). In addition, to obtain the tidal mixing effect, we considered 10 major tidal and tidal current harmonic components (M_2, S_2, N_2, K_2, K_1, O_1, P_1, Q_1, M_f, and M_m) from TPX07 (Egbert and Erofeeva, 2002). The GLS vertical mixing scheme was used for parameterization (Umlauf and Burchard, 2003). The bottom stress is parameterized with a quadratic drag las using a drag coefficient (2.5×10^{-3}), and horizontal viscosity and diffusion coefficients are 25 m^2 s^{-1} and 50 m^2 s^{-1}, respectively.

In this study, the model domain (105–170° E, 13–52° N) is the Northwest Pacific (NWP), which is one of the key regions for conducting global air–sea gas exchange, and includes the East Sea, Yellow Sea, East China Sea, and South China Sea (Fig. 2). The horizontal resolution is 1/12°, both in longitude and latitude and the number of vertical layers is 50. The bottom topography from GEBCO data (Weatherall et al. 2015) is interpolated onto the model grid. NPRT was operated for a total of 15 years (2000–2014). To address the requirement for a sufficiently long spin-up time for executing the biogeochemical model, we conducted an additional spin-up for the initial five years. Therefore, in this study, the model results averaged over the last 10 years were used for the analysis.

NPRT simulations were evaluated and analyzed by comparing them with available observational data. SSH distribution was obtained from the Copernicus Marine Environment Monitoring Service (CMEMS) satellite data from 2005 to 2014. In addition, to evaluate the reproducibility of chlorophyll concentrations, the Moderate Resolution Imaging Spectroradiometer (MODIS) and the Coupled Model Intercomparison Project phase 6 (CMIP6; Eyring et al. 2016) were employed. As shown in Table1, this study adopted six models from CMIP6, providing chlorophyll concentrations for the historical period (2005–2014). Each model is a single ensemble member, typically the ‘r1i1p1f1’. For dissolved oxygen

https://doi.org/10.5194/egusphere-2024-1509
Preprint. Discussion started: 22 October 2024

and nutrients, we used the annual and monthly climatological datasets from the World Ocean Atlas 2018 (WOA18) at a horizontal resolution of 1° × 1°. In addition, we utilized the conductivity–temperature–depth (CTD) measurement data such as DO, from the Japan Meteorological Agency (JMA) along the 137° E line from 2005 to 2014. The simulated DIC in NPRT was compared with observational data from the Global Ocean Data Analysis Project version 2 (GLODAPv2; Lauvset et al., 2016) with a horizontal resolution of 1° × 1° and 33 vertical layers from 0 to 5,500 m. GLODAPv2 is the mapped climatology fields averaged from 1972 to 2013 at the Carbon Dioxide Information Analysis Center (CDIAC).

3. Results

3.1. Physics

The study area includes the KOE, the East/Japan Sea (hereafter East Sea), and the Yellow and East China Seas (YECS), which are greatly influenced by tidal mixing and riverine effects. Each region is characterized by diverse oceanic environments, which determine the biogeochemical characteristics. For example, in the KOE, the distributions of biogeochemical variables are determined by various physical and biological processes, such as advection, horizontal mixing, vertical mixing, photosynthesis, and respiration. In particular, the YECS is a river-dominated marginal sea, where large amounts of nutrients are discharged into the sea along with freshwater (Dai et al., 2022; Na et al., 2024). Therefore, to accurately simulate the biogeochemical properties, validating the oceanic physical characteristics, such as water temperature, current, and salinity, is necessary. The distribution of ocean currents, in conjunction with water temperature and salinity, is essential for determining the oceanic physical characteristics. This key factor plays a fundamental role in direct and indirect assessments of all aspects of the marine environment. To validate the reproducibility of the physical characteristics, the simulated SSH data were compared with satellite-observed altimetry data from CMEMS.

Fig. 3 shows the long-term mean SSH distributions in CMEMS and NPRT during 2005–2014. The Kuroshio Current originates from east of the Philippine coast, where it flows northeastward, passes through the Tokara Strait, and continues eastward, meandering along the southern coast of Japan. Furthermore, in the Shikoku Basin, there is a long-standing anticyclonic eddy associated with ocean-bottom topography (Ding et al., 2022). In the subarctic region, the Oyashio Current flows southward and converges with the Kuroshio Current, resulting in the mixing of distinct water masses; the region where this happens is known as Kuroshio–Oyashio Confluence Region (142–160° E, 35–40° N; Sugimoto and Hanawa, 2011; Zhu et al., 2019). As mentioned previously, the NPRT results generally

https://doi.org/10.5194/egusphere-2024-1509
Preprint. Discussion started: 22 October 2024

agree well with the observed characteristics of the upper-layer circulation system in the NWP.

Sea water temperature is not only one of the key factors contributing to the growth of phytoplankton but also an important physical factor that determines the water mass distribution in the ocean. In this study, the water temperature simulated from NPRT was verified using long-term averaged WOA18 data. Fig. 4 shows the sea surface temperature (SST) in WOA18 and NPRT for annual means, winter, and summer. The Northwest Pacific exhibits subtropical characteristics, with year-round high temperatures above 25 °C approximately 20° N. Between 20° N and 35° N, a seasonal temperature variation of over 8 °C is observed between winter and summer. Additionally, this region is predominantly influenced by the Kuroshio Current with warm water mass, which results in the northward distribution of isotherms along the Japanese coast. As mentioned above, a significant north–south temperature gradient is observed between 35° N and 40° N, corresponding to the Kuroshio–Oyashio Confluence Region. The characteristics of the SST distribution in the Northwest Pacific are highly pronounced in NPRT. Notably, the location of the Kuroshio–Oyashio Confluence Region, which plays a crucial role in the formation of the North Pacific Intermediate Water (NPIW), is also accurately simulated.

The NPIW is formed in the Kuroshio–Oyashio Confluence Region; from there, it spreads into the NWP. The NPIW is characterized by salinity and potential vorticity minima, with its primarily distributed between density 26.6 and 27.2 σ_θ, corresponding to depths of 600–800 m (Lembke-Jene et al., 2017). The NPIW transports large amounts of nutrients to the NWP. Therefore, simulating the NPIW is important for the reproduction of biogeochemical characteristics in the NWP. Comparing the vertical structures of zonal mean salinity between 140° and 160° E to those in the WOA18 data shows that the depth of the salinity minimum layer is approximately 600–800 m, similar to the observational data (Fig. 5). However, the salinity minimum layer is about 0.2 psu higher than that of the observations. This is attributed to the insufficient model integration time, resulting in inadequate dispersion of the NPIW. Nevertheless, NPRT adequately reproduces not only the surface currents but also the ventilation for the formation of the NPIW.

The YECS are characterized by the dominant effects of tidal mixing and runoff. Freshwater discharged from the Yangtze River, one of the major sources of nutrients in the East China Sea, forms a low-salinity plume that spreads and influences the stratifications of the surrounding areas (Moon et al., 2009). NPRT did not include all rivers in the YECS; nevertheless, a total of 12 rivers, including the Yangtze River, were included (Fig. 2). Regarding the oceanographic characteristics of the YECS, the model exhibits similar patterns with those of the observations from WOA18, despite of a negative bias (Fig. 6). During winter (February; Fig. 6e), the simulated sea surface salinity distribution in the YECS is below 32.0 psu, whereas during the freshwater discharge-intensive summer (August; Fig. 6f), the salinity drops below 30 psu, forming a low-salinity tongue shaped feature extending toward the Korean coast. In the NWP, high salinity water (> 34.0 psu) extends northward to around 40° N during winter and around 35° N during summer. The reproduced distinct seasonal variability is similar to that in the WOA18 data, with all spatial correlation coefficients and root-mean-square error (RMSE) for surface salinity distribution in the annual mean, winter, and summer being over 0.93 and 0.33–0.42 psu.

Overall, NPRT reasonably simulates the major characteristics observed in each region and is, therefore, suitable for analyzing the spatiotemporal distribution and characteristics of chlorophyll concentration, nutrients, and the carbon cycle influenced by these physical properties.

3.2. Biogeochemistry

3.2.1 Chlorophyll

The characteristics of the simulated chlorophyll distribution were compared with those inferred from MODIS satellite data (Fig. 7). The chlorophyll concentrations derived from satellite data contain both the sea surface and mixed layer components due to the backscattering effect of reflected light (Park et al., 2014, Jung et al., 2019; Jochum et al., 2019). Therefore, in this study, 0–20 m depth-averaged chlorophyll concentrations from NPRT were compared with satellite data for 2005–2014. In addition, we analyzed the characteristics of the high-resolution regional model (NPRT) compared to the global biogeochemical models in CMIP6 datasets. Biogeochemical models include various variables, among which chlorophyll concentration is influenced by physical factors (temperature and circulation system), light, and various nutrients, and it exhibits distinct seasonal variability. Moreover, since it is observed via satellite, the observational uncertainty is lower than other nutrients, making it easier to objectively analyze the characteristics of biogeochemical models. We considered it as a representative variable for evaluating the performance of biogeochemical models and used a total of 13 ensemble members in CMIP6 models (Table 1). Of the 13 members (Table 1), ensemble numbers 1 to 8 were calculated using the 0–20 m depth averaged chlorophyll concentration, while the remaining ensembles only provided surface data.

Since the chlorophyll distribution and seasonal variation have exhibit different characteristics in each region, the analysis in this study was divided into the NWP, East Sea, and YECS. First, analyzing the NWP and East Sea, the chlorophyll concentrations generally increase from low to high latitudes according to observation (Fig. 7a). Seasonal variability is generally highest in spring (April), decreases gradually during summer, and then increases again in autumn (October and November) in the East Sea

https://doi.org/10.5194/egusphere-2024-1509
Preprint. Discussion started: 22 October 2024

and NWP (Fig. 8a, b). The phytoplankton bloom in spring is driven by increased nutrient input from the subsurface owing to vertical mixing during winter, enhanced solar radiation, and atmospheric nutrient deposition, particularly from spring dust storms in the NWP, including the East Sea (Son et al., 2014; Jo et al., 2007). Another bloom occurs in autumn after the gradual weakening of the strong stratification in summer, leading to the re-input of nutrients from the subsurface. However, the autumn bloom is typically weaker than the spring bloom because the light conditions and water temperatures are not favorable for phytoplankton growth (Chen et al., 2022). In NPRT, the distribution of the annual mean chlorophyll concentration is similar to that of observation in the NWP and East Sea (pattern correlation: 0.72 and 0.61, respectively), except in the YECS (pattern correlation: 0.45). The seasonal characteristics were well reproduced by NPRT (Fig. 8a, b). Despite the positive biases in the chlorophyll concentration distributions throughout the seasons in the NWP and East Sea, as represented in NPRT, the seasonal variation of the chlorophyll concentration was similar to observation (Fig. 8). Most of the results in CMIP6 models do not adequately capture the autumn peak in the NWP and East Sea, and exhibit a negative bias compared with the results of MODIS and NPRT (Fig. 8). The pattern correlation ranges of the annual mean chlorophyll concentrations for each ensemble member of CMIP6 in the NWP and East Sea are -0.06–0.61, -0.15–0.17, respectively (Fig. 9). Some models in the CMIP6 datasets show negative pattern correlation.

The YECS exhibited higher chlorophyll concentrations than did the NWP (Fig 7a, b), primarily due to nutrient inputs from numerous rivers (Zhou et al., 2008), and the peak appeared in spring and increase from summer (Fig. 8c). In summer, biomass blooms occur around the mouths of the Yangtze River because of discharge of freshwater and significant amounts of nutrients into the ocean (Gong et al., 2003). In global biogeochemical models, riverine effects are typically assessed using the surface flux method. Riverine effects tend to weaken, resulting in a tendency for global biogeochemical models to inadequately reproduce chlorophyll structures near river estuaries. To address this issue, in this study, freshwater discharge and nutrients were considered simultaneously, following an approach similar to that adopted in the regional biogeochemical model. However, the chlorophyll concentrations in NPRT still tend to be underestimated (RMSE: 1.62 μmol kg^{-1}) in the YECS, including the Yangtze River estuary (Fig. 7c). This can be attributed to the incomplete consideration of the influences exerted by numerous rivers along the Chinese and Korean coasts as well as the utilization of default data provided by MOM GitHub, which deviates from the actual diverse biogeochemical variables (Alk, LITH, NH_4, NO_3, and Fed) introduced from the atmosphere. Nonetheless, NPRT effectively captures the spatial patterns for the annual mean distribution (pattern correlation: 0.45; Fig. 9d) and the seasonal variability, i.e., biomass blooms, near the Yangtze River and along the Chinese coast, driven by large freshwater discharge (Fig. 7). However, in the case of the CMIP6 models, negative bias is dominant regardless of

https://doi.org/10.5194/egusphere-2024-1509
Preprint. Discussion started: 22 October 2024

the season (Fig. 8c), and they also lack clear seasonal variability in the chlorophyll concentration, which typically increases beginning in summer (Fig. 8). Based on the model results, the high-resolution regional model exhibits biases specific to each region but effectively reproduces seasonal variability that is not captured by the global low resolution model.

Through analysis of the Taylor diagrams (Taylor 2001), which assess the spatial correlation between observational data and model results, the results in NPRT are better than those from CMIP6 in the NWP and East Sea (Fig. 9). The Taylor diagram score (TD score; Taylor, 2001; Jin et al. 2023) is calculated in each region using the below formulation.

$$TD(Taylor\ diagram)\ Score = |1-R| + \left|1-\frac{\sigma_M}{\sigma_O}\right| + \frac{E'}{\sigma_O}\ , \qquad (3)$$

where R is the pattern correlation, σ_M and σ_O indicate the standard deviations in model and observation. E' is the RMSE. The TD scores in NPRT are lower than those in CMIP6, especially, in the East Sea, the reproducibility of the chlorophyll concentration distribution has significantly improved (Table 2). The TD score in NPRT is also better than that of each ensemble data in CMIP6 in the YECS, which is influenced by river discharge. For each region (the NWP, EJS, YECS), by analyzing the Taylor diagram with each ensemble model data, it can be confirmed that NPRT results have improved compared to the CMIP6 in all regions (Fig. 9).

3.2.2 Nutrients

The results of the simulated nitrates, phosphates, and silicates, which are essential for the growth of phytoplankton, were compared with the results of the observationally base WOA18 climatology (Fig. 10). Fig. 10a, d shows the comparison of the simulated surface annual mean nitrates with the observed ones. The distribution of the annual mean surface nitrate concentration in the observational data reveals a characteristic increase from low to high latitudes, with concentrations exceeding 15 μmol kg^{-1} in the subarctic region (Fig. 10a). In the model results, the annual mean concentration of nitrate also increases with increasing latitude and is predominantly distributed in the East Sea, Okhotsk Sea, and the Oyashio extension region (Fig. 10d). Compared with that in the observations, the overall distribution of nitrate concentrations is underestimated (Fig. 10g). In particular, in the subarctic region, the model results exhibit a large negative bias of over -10 μmol kg^{-1}, whereas in the East Sea and the Kuroshio and its extension regions, it exhibits a positive bias. The pattern correlation and RMSE in the study area are 0.83 and 5.70 μmol kg^{-1}, respectively. The simulated surface nitrate concentrations exhibit a clear seasonal variability, similar to that in the WOA18 data (Fig. 11a). In winter, high nitrate concentrations distributed in the subsurface are supplied to the surface by vertical mixing, resulting in an increase in the upper–layer nitrate concentration from winter to spring. In summer and autumn, a distinct seasonal

https://doi.org/10.5194/egusphere-2024-1509
Preprint. Discussion started: 22 October 2024

variability is observed, with concentrations gradually decreasing owing to enhanced stratification.

The distribution of the annual-mean phosphates in NPRT is similar to that in WOA18 (pattern correlation: 0.83; Fig. 10b, e). However, there is a negative bias in the subarctic region and a positive bias in the eastern coast of Sakhalin and East Sea (Fig. 10h). The bias range is approximately -1.2–0.5, and the RMSE is approximately 0.53 μmol kg^{-1}. Unlike other nutrients, the simulated silicate exhibits a significant positive bias (> 30 μmol kg^{-1}) and a negative bias (> 30 μmol kg^{-1}) in the YECS and the subarctic region, respectively (Fig. 10i). The TOPAZ module is suitable for analyzing the biogeochemical environment in the ocean; however, the reproducibility of its results in marginal seas, such as the YECS, where riverine and tidal effects are important, might be limited. Therefore, for accurate reproduction, it is necessary to adjust various parameters based on precise river discharge data. Despite significant biases, all nutrients analyzed in this study exhibit clear seasonal variabilities, with maximum concentrations occurring in winter and minimum concentrations occurring in summer (Fig. 11).

The vertical errors of the zonally averaged annual mean nutrients (nitrate and phosphate) in the NWP were overestimated south of the Kuroshio–Oyashio Confluence Region (40° N) until a depth of 500 m (Fig. 12). However, in the 500–1500 m, the underestimation error in the 500–1500 m appears, which seems to be related to the NPIW simulation. In the intermediate layer of the NWP, the subarctic intermediate water nutrient pool (SINP) with high nutrient concentrations appears along with the NPIW formed in the Kuroshio–Oyashio Confluence Region (Nishioka et al., 2020; 2021). However, it is considered that the SNIP is not distinct in NPRT due to the negative bias in the subarctic region, which is the source of the SNIP.

3.2.3 Dissolved Inorganic Carbon

DIC is a crucial component of ocean biogeochemistry and is directly linked to plankton photosynthesis and respiration; hence, it is a valuable parameter for the analysis of the carbon system (Ding et al., 2018). The results of NPRT, averaged from 2005 to 2014, were compared with observed climatological data obtained from GLODAPv2 (Fig. 13). For both the model results and observational data, the annual mean surface DIC in the subarctic region is significantly higher than that in the subtropical region. The simulated annual mean surface DIC in NPRT generally exhibits a positive bias, except in the YECS and around the Pearl River estuary, where there is a significant negative bias of over -300 μmol kg^{-1}. The bias range for the entire study area is approximately between -650 and 180 μmol kg^{-1}, with a pattern correlation of approximately 0.41 and RMSE of 99.84 μmol kg^{-1}. Excluding the YECS, the pattern correlation and RMSE are approximately 0.81 and 95.67 μmol kg^{-1}, respectively. The surface DIC concentration in the NWP generally exhibits seasonal variability (Fig. 15), increasing in winter due to vertical mixing and high solubility, and decreasing in summer. NPRT reasonably reproduces the seasonal variability, revealing maxima in March and minima in September (or August in the YECS), and the amplitude of the seasonal change in the simulated surface DIC exceeds 50 μmol kg^{-1} (Fig. 15), especially in the East Sea, where the amplitude is approximately 100 μmol kg^{-1}. Ishizu et al. (2021) suggested that DIC concentrations are predominantly influenced by factors such as the advection, horizontal/vertical mixing, biological processes, and air–sea exchange, depending on latitude and depth. In particular, for the surface DIC concentration, regardless of the latitude, the air–sea exchange and vertical mixing are balanced. To improve the spatiotemporal biases, it is necessary to consider factors such as vertical mixing, air–sea exchange, and water temperature that influence DIC concentrations in NPRT.

When comparing the vertical structures of the zonally averaged annual-mean DIC concentration in the NWP (Fig. 14), the positive bias still appears large (with a maximum value of 130 μmol kg^{-1} at a depth of 300 m) in the upper 600 m; however, the vertical structures of DIC closely resemble the observations in the NWP. Nevertheless, near the Yangtze River estuary, where a large amount of freshwater is discharged, NPRT shows a significant negative bias in the DIC distribution below 1,900 μmol kg^{-1} compared to that of the observational data from GLODAPv2. The model results, which are consistent with observational data from ships, are associated with low DIC input from rivers (Wang et al., 2016). This characteristic can be due to the use of a high-resolution regional biogeochemical model.

3.2.4 Dissolved Oxygen

DO is important for analyzing the ecological and physical characteristics of marine ecosystems and serves as a tracer. It is associated with ocean temperature, air–sea exchange, and phytoplankton photosynthesis. The simulated DO results were compared with the WOA18 climatological data and observations from the JMA (Figs. 16 and 17). Both the observations (i.e., WOA18) and the model results demonstrate a typical increase in surface DO concentrations from low to high latitudes, with high concentrations of DO more than 300 μmol kg^{-1} being distributed in the Okhotsk Sea and the Oyashio region (Fig. 16). With respect to that of the WOA18 observations, the model tends to underestimate DO exhibiting a dominant negative bias (up to approximately -30 μmol kg^{-1}) in the Oyashio region. The pattern correlation and the RMSE of DO concentration between the model results and WOA18 data are 0.99 and 9.99 μmol kg^{-1}, respectively. To compare the vertical structures of DO, ship measured DO data from the JMA were employed along the 137° E line across the Kuroshio main path in January and June (Fig. 17). Both the observations and the model results show the presence of an oxycline layer, where the DO decreases sharply with depth. Below this layer, DO minimum zone is evident. However, the depth of the DO minimum zone in NPRT appears below 500

https://doi.org/10.5194/egusphere-2024-1509
Preprint. Discussion started: 22 October 2024

m regardless of the season, similar to the observations (JMA); however, the minimum DO concentrations are approximately 25 μmol kg^{-1} higher than the JMA data. This is presumed to be caused by the weak NPIW formation. These characteristics are also evident in the results obtained using the TOPAZ module (Lee et al., 2022). Consequently, NPRT adequately qualitatively reproduces the spatiotemporal distribution of the DO circulation system. However, sufficient observational data, accurate initial and boundary conditions, and adequate spin-up times are required for quantitative and reproducibility improvements, particularly in the intermediate layer.

4. Conclusions and discussion

Recently, there has been a significant increase in interest in oceanic physical characteristics, marine ecosystems, and carbon cycling. The coupled physical–biogeochemical ocean model developed in this study, namely ROMS–TOPAZ (NPRT v1.0), is a preliminary investigation that reflects the characteristics of local regions with high resolution, enabling analysis of the interactions between the physical and biogeochemical processes in the ocean. The study area comprised the NWP, East Sea and YECS, exhibiting diverse characteristics depending on the region. The study area is one of the main regions where nutrients are consumed by primary production. The CO_2 exchange between air and sea is dominant in the NWP (Takahashi et al., 2009; Ishizu et al., 2020); however, in the YECS, the biogeochemical environment is significantly influenced by riverine discharge (Zhou et al., 2008). In these oceanic regions with such diverse features, we evaluated the reproducibility of the spatial distribution and seasonal variability of physical and biogeochemical variables derived using NPRT. To generate the initial and boundary data for the biogeochemical variables required to simulate NPRT, first, MOM5–TOPAZ was integrated for 100 years under the pCO_2 environment and ERA5 of year 2000 and then was conducted for an additional 15 years under actual atmospheric CO_2 concentration conditions (2000–2014). Using the biogeochemical variables reproduced by MOM5–TOPAZ and the physical variables from HYCOM, NPRT was subsequently integrated for 15 years (2000–2014). In this study, model results from the last 10 years (2005–2014) were used in the analysis.

NPRT successfully reproduced the overall spatial distributions, such as upper-layer circulation, the NPIW formation via ventilation, and salinity in the YECS influenced by freshwater input, as well as the seasonal variability of biogeochemical variables. For chlorophyll concentration, although NPRT showed positive and negative biases in the study area, it effectively reproduced not only the seasonal variation in the NWP, East Sea, and the YCES, but also showed improved TD scores in all regions have improved compared to the CMIP6 data. In addition. in the YECS, because a significant amount of nutrients is discharged from the Yangtze River along with a large amount of freshwater, leading to

https://doi.org/10.5194/egusphere-2024-1509
Preprint. Discussion started: 22 October 2024

biomass blooms around the Yangtze River estuary, the chlorophyll concentrations start to increase from July. As a result, low DIC concentrations associated with river effects were also simulated around the Yangtze River. Such regional characteristics are difficult to reproduce using low-resolution global models.

For nutrients (nitrate, phosphates, and silicate), there was generally a positive bias in winter and a negative bias in summer; however, the spatial patterns were also overall well simulated. The overall biases for nutrients (nitrate and phosphate) were small except for silicate, and the pattern correlations were approximately 0.5–0.7. The reason for the large biases simulated in NPRT is the significant uncertainty persisting in the initial and boundary data of the biogeochemical variables generated from MOM5–TOPAZ, when compared with observations. In particular, in regions greatly influenced by freshwater input, such as the YECS, significant biases may arise owing to various factors such as river discharge, nutrient supply, vertical mixing processes, and atmospheric forcing. The results reproduced in this study cannot be easily improved, because it is difficult to acquire and utilize freshwater discharge and nutrient concentrations from all rivers in the YECS. To address these issues, it is necessary to minimize the uncertainty of biogeochemical variables through various sensitivity experiments and analyses, including not only the use of open boundary and initial data, but also parameter adjustment.

In summary, the coupled model NPRT developed in this study is an important tool for studying the interactions between ocean physics and biogeochemistry at a high resolution, enabling research on a regional scale. In the future, this tool is expected to provide a basis for understanding the mechanisms of oceanic physics and biogeochemical environments in various regions, ultimately improving the accurate assessment and predictability of carbon cycling.

https://doi.org/10.5194/egusphere-2024-1509
Preprint. Discussion started: 22 October 2024

Acknowledgments.

This work has been supported by Basic Science Research Program through the National Research Foundation of Korea (NRF) funded by the Ministry of Education (RS-2024-00451970 and RS-2024-00461585), and the National Research Foundation of Korea (NRF) grant funded by the Korea government (MIST) (NRF-2022M3I6A1086449). The main calculations were performed by using the supercomputing resource of the Korea Meteorological Administration (National Center for Meteorological Supercomputer).

Code Availability.

ROMS–TOPAZ (NPRT v1.0) used in this study is archived on Zenodo (https://doi.org/10.5281/zenodo.11218350). In addition, the input data (initial, boundary, atmospheric forcings, atmospheric deposition data) for conducting NPRT and the model results are archived on Zenodo (https://zenodo.org/records/13941078).

Data availability statement.

The data analyzed in this study are available from public websites. Bathymetric data were provided by GEBCO (GEBCO Compilation Group, 2021; GEBCO_2021 Grid, https://doi.org/10.5285/c6612cbe-50b3-0cffe053-6c86abc09f8f, GEBCO, 2022, last access: 1 March 2023). The atmospheric forcings were provided by ECMWF Reanalysis v5 (ERA5; https://cds.climate.copernicus.eu/cdsapp#!/search?type=dataset:1 March 2023). For conducting the MOM–TOPAZ model, the input data for initial, boundary, and dry/wet atmospheric deposition were provided by MOM GitHub (https://mom-ocean.github.io/docs/quick-start-guide/, last access: 1 March 2023). For conducting NPRT, the physical ocean initial and boundary data were used from Hybrid Coordinate Ocean Model (HYCOM; https://tds.hycom.org/thredds/catalog.html:1 December 2023). The SSH data were obtained from the Copernicus Marine and Environment Monitoring Service (CMEMS; http://marine.copernicus.eu, last access: 15 November 2023). The data used to evaluate the model results in this study are freely available online from Japan Meteorological Agency (JMA; https://www.data.jma.go.jp/gmd/kaiyou/db/vessel_obs/data-report/html/ship/ship_e.php), World Ocean Atlas 2018 (WOA18; https://www.ncei.noaa.gov/access/world-ocean-atlas-2018), , Moderate Resolution Imaging Spectroradiometer (MODIS; http://www.daac.gsfc.nasa.gov/data/dataset/ MODIS/) for chlorophyll concentration, and GLODAPv2 (GLODPAv2; (https://www.ncei.noaa.gov/access/ocean-carbon-acidification-data-system/ oceans/GLODAPv2_2022) for dissolved inorganic carbon. The CMIP6 model datasets are freely available online (https://aims2.llnl.gov/search/cmip6, last access: 1 December 2023).

Author Contribution.

DK, HCJ, and JHM designed the study. DK and HCJ conducted the models and the simulations and primarily responsible for developing ROMS–TOPAZ (NPRT v1.0). NHL analyzed CMIP6 data. All authors analyzed and discussed the results and contributed to writing and editing of the article.

Competing interests.

The authors declare that they have no conflict of interest.

https://doi.org/10.5194/egusphere-2024-1509
Preprint. Discussion started: 22 October 2024

References

Arakawa, A. and Lamb, V. R.: Computational design of the basic dynamical processes of the UCLA general circulation model, in: General circulation models of the atmosphere, Meth. Comput. Phys., edited by: Chang, J., Elsevier, 17, 173–265, https://doi.org/10.1016/B978-0-12-460817-7.50009-4, 1977.

Chen, S., Meng, Y., Lin, S., and Xi, Ji.: Remote sensing of the seasonal and interannual variability of surface chlorophyll-a concentration in the Northwest Pacific over the past 23 years (1997-2020), Remote Sens., 14, 5611, https://doi.org/10.3390/rs14215611, 2022.

Chierici, M., Fransson, A., and Nojiri, Y.: Biogeochemical processes as drivers of surface fCO_2 in contrasting provinces in the subarctic North Pacific Ocean, Global Biogeochem. Cycles, 20, GB1009, https://doi.org/10.1029/2004GB002356, 2006.

Dai, M., Su, J., Zhao, Y., Hofmann, F. E., Cao, Z., Cai, W.-J., Gan, J., Lacroix, F., Laruelle, G. G., Meng, F., Müller, D., Regnier, P. A.G., Wang, G., and Wang, Z.: Carbon fluxes in the coastal ocean: synthesis, boundaty processes, and future trends, Annu. Rev. Earth Planet. Sci., 50, 593-626, https://doi.org/10.1146/annurev-earth-032320-090746, 2022.

Ding, L., Ge, T., Gao, H., Luo, C., Xue, Y., Druffel, E.R.M., and Wang, X.: Large variability of dissolved inorganic radiocarbon in the Kuroshio extension of the Northwest North Pacific, Radiocarbon, 60, 691–704, https://doi.org/10.1017/RDC.2017.143, 2018.

Ding, Y., Yu, F., Ren, Q., Nan, F., Wang, R., Liu, Y., and Tang, Y.: The physical-biogeochemical responses to a subsurface Anticyclonic eddy in the northwest Pacific. Front. Mar. Sci. 8. https://doi.org/10.3389/fmars.2021.766544, 2022.

Dunne, J. P., Armstrong, R. A., Gnanadesikan, A., and Sarmiento, J. L.: Empirical and mechanistic models for the particle export ratio, Global Biogeochem. Cycles, 19, GB4026, https://doi.org/10.1029/2004GB002390, 2005.

Dunne, J. P., Sarmiento, J. L., and Gnanadesikan, A.: A synthesis of global particle export from the surface ocean and cycling through the ocean interior and on the seafloor, Global Biogeochem. Cy., 21, GB4006, https://doi.org/10.1029/2006GB002907, 2007.

Dunne, J. P., John, J. G., Adcroft, A. J., Griffies, S. M., Hallberg, R. W., Shevliakova, E., Stouffer, R. J., Cooke, W., Dunne, K. A., Harrison, M. J., Krasting, J. P., Malyshev, S. L., Milly, P. C. D., Phillipps, P. J., Sentman, L. T., Samuels, B. L., Spelman, M. J., Winton, M., Wittenberg, A. T., and Zadeh, N.: GFDL's ESM2 Global Coupled Climate–Carbon Earth System Models. Part I: Physical Formulation and Baseline Simulation Characteristics, J. Climate, 25, 6646–6665, https://doi.org/10.1175/jcli-d11-00560.1, 2012.

Egbert, G. D. and Erofeeva, S. Y.: Efficient inverse modeling of barotropic ocean tides, J. Atmos. Ocean. Technol., 19, 183–204, https://doi.org/10.1175/1520-0426(2002)019<0183:EIMOBO>2.0.CO;2, 2002.

Eyring, V., Bony, S., Meehl, G. A., Senior, C. A., Stevens, B., Stouffer, R. J., and Taylor, K. E.: Overview of the Coupled Model Intercomparison Project Phase 6 (CMIP6) experimental design and organization, Geosci. Model Dev., 9, 1937–1958, https://doi.org/10.5194/gmd-9-1937-2016, 2016.

Fairall, C. W., Bradley, E. F., Rogers, D. P., Edson, J. B., and Young, G. S.: Bulk parameterization of air-sea fluxes for tropical oceanglobal atmosphere Coupled-Ocean Atmosphere Response Experiment, J. Geophys. Res., 101, 3747–3764, https://doi.org/10.1029/95JC03205, 1996.

Gong, G.-C., Wen, Y.-H., Wang, B.-W., and Liu, G.-J.: Seasonal variation of chlorophyll a concentration, primary production and environmental conditions in the subtropical East China Sea, Deep Sea Res. II, 50, 1219-1236, https://doi.org/10.1016/S0967-0645(03)00019-5, 2003.

Hanawa, K., and Mitsudera, H.: Variation of water system distribution in the Sanriku coastal area, J. Oceanogr. Soc. Jap., 42, 435-446, https://doi.org/10.1007/BF02110194, 1987.

https://doi.org/10.5194/egusphere-2024-1509
Preprint. Discussion started: 22 October 2024

Hauri, C., Schultz, C., Hedstrom, K., Danielson, S., Irving, B., Doney, S. C., Dussin, R., Curchitser, E. N., Hill, D. F., and Stock, C. A.: A regional hindcast model simulating ecosystem dynamics, inorganic carbon chemistry and ocean acidification in the Gulf of Alaska, Biogeosciences, 17, 3837-3857, https://doi.org/10.5194/bg-17-3837-2020, 2020.

Hersbach, H., Bell, B., Berrisford, P., Hirahara, S., Horányi, A., Muñoz-Sabater, J., Nicolas, J., Peubey, C., Radu, R., Schepers, D., Simmons, A., Soci, C., Abdalla, S., Abellan, X., Balsamo, G., Bechtold, P., Biavati, G., Bidlot, J., Bonavita, M., De Chiara, G., Dahlgren, P., Dee, D., Diamantakis, M., Dragani, R., Flemming, J., Forbes, R., Fuentes, M., Geer, A., Haimberger, L., Healy, S., Hogan, R. J., Hólm, E., Janisková, M., Keeley, S., Laloyaux, P., Lopez, P., Lupu, C., Radnoti, G., de Rosnay, P., Rozum, I., Vamborg, F., Villaume, S., and Thépaut, J.-N.: The ERA5 global reanalysis, Q. J. Roy. Meteor. Soc., 146, 1999– 2049, https://doi.org/10.1002/qj.3803, 2020 Ishizu, M., Miyazawa, Y., Tsunoda, T., and Guo, X.: Seasonal variability in the inorganic ocean carbon cycle in the Northwest Pacific evaluated using a biogeochemical and carbon model coupled with and operational ocean model, Clim. Change, 162, 877-902, https://doi.org/10.1007/s10584-020-02779-2, 2020.

Ishizu, M., Miyazawa, Y., and Guo, X.: Long-term variations in ocean acidification indices in the northwest Pacific from 1993 to 2018, Clim Change, 168, https://doi.org/10.1007/ s10584-021-03239-1, 2021.

Jin, S., Wei, Z., Wang, D., and Xu, T.: Simulated and projected SST of Asian marginal seas based on CMIP6 models, Front. Mar. Sci., 10:1178974, https://doi.org/10.3389/fmars.2023.1178974, 2023.

Jo, C.O., Lee, J.-Y., Park, K.-A., Kim, Y.H., and Kim, K.-R.: Asian dust initiated early spring bloom in the northern East/Japan Sea, Geophy. Res. Lett., 34, L05602, https://doi.org/10.1029/2006GL027395, 2007

Jochum, M., Yeager, S., Lindsay, K., Moore, K., and Murtugudde, R.: Quantification of the feedback between phytoplankton and ENSO in the community climate system model, J. Clim., 23, 2916–2925, https://doi.org/10.1175/2010JCLI3254.1, 2009.

Jung, H. K., Rahman, S. M., Kang, C.-K., Park, S.-Y., Lee, S. H., and Park, H. J.: The influence of climate regime shifts on the marine environment and ecosystems in the East Asian Marginal Seas and their mechanism, Deep-Sea Res. II, 143, 110-120, https://doi.org/10.1016/j.dsr2.2017.06.010, 2017.

Jung, H.-C, Moon, B.-K., Lee, H., Choi, J.-H., Kim, H.-K., Park, J.-Y., Byun, Y.-H., Lim, Y.-J., and Lee, J.: Development and assessment of NEMO(v3.6) –TOPAZ(v2), a coupled global ocean biogeochemistry model, Asia-Pac. J. Atmos. Sci., 56, 411-428, https://doi.org/10.1007/s13143-019-00147-4, 2020.

Kang, X., Zhang, R.H., Gao, C., and Zhu, J.: An improved ENSO simulation by representing chlorophyll-induced climate feedback in the NCAR community earth system model, Sci. Rep., 7, 1-9, https://doi.org/10.1038/s41598-017-17390-2, 2017.

Kawai., H.: Hydrography of Kuroshio extension, in: Kuroshio: Its Physical Aspects, edited by: Stommel, H. and Yoshida, K., University of Tokyo Press, 235–352, 1972.

Kuroda, H., Toya, Y., Watanabe, T., Nishioka, J., Hasegawa, D., Taniuchi, Y., and Kuwata, A.: Influence of Coastal Oyashio water on massive spring diatom blooms in the Oyashio area of the North Pacifc, Ocean. Prog Oceanogr., 175, 328–344. https://doi.org/10.1016/j.pocean.2019.05.004, 2019.

Kwon, K.M.: A numerical experiment on the currents along the eastern boundary of the Yellow Sea in summer 2007. M.D Thesis, Kunsan National University, 89p.

Large, W. G., McWilliams, J. C., and Doney, S. C.: Ocean vertical mixing: a review and a model with a nonlocal boundary layer parameterization, Rev. Geophys., 32, 363–403, https://doi.org/10.1029/94RG01872, 1994.

Large, W.G., and Yeager, S.G.: The global climatology of an interannually varying air-sea flux data set. Clim. Dyn. 33, 341–364, https://doi.org/10.1007/s00382-008-0441-3, 2009.

Lauvset, S. K., Key, R. M., Olsen, A., van Heuven, S., Velo, A., Lin, X., Schirnick, C., Kozyr, A., Tanhua, T., Hoppema, M., Jutterström, S., Steinfeldt, R., Jeansson, E., Ishii, M., Perez, F. F., Suzuki, T., and Watelet, S.: A new global interior ocean mapped climatology: the 1° × 1° GLODAP version 2, Earth Syst. Sci. Data, 8, 325–340, https://doi.org/10.5194/essd-8-325-2016, 2016.

Lee, H., Moon, B.-K., Jung, H.-C., Park, J.-Y., Shim, S., La, N., Kim, A.-H., Yum, S.S., Ha, J.-C., Byun, Y.-H.,

https://doi.org/10.5194/egusphere-2024-1509
Preprint. Discussion started: 22 October 2024

Sung, H.M., and Lee, J.: Development of the UKESM-TOPAZ Earth System Model (Version 1.0) and preliminary evaluation of its biogeochemical simulations, Asia-Pac. J. Atmos. Sci., 58(3), 379-400, https://doi.org/10.1007/s13143-021-00263-0, 2022.

Lembke-Jene, L, Tiedemann, R., Nürnberg, D., Kokfelt, U., Kozdon, R., Max, L., Röhl, U., and Gorbarenko, A.: Deglacial variability in Okhotsk Sea Intermediate Water ventilation and biogeochemistry: Implications for North Pacific nutrient supply and productivity, Quat. Sci. Rev., 160, 116-137, https://doi.org/10.1016/j.quascirev.2017.01.016, 2017.

Ma, S., Tian, Y., Li, J., Yu, H., Cheng, J., Sun, P., Fu, C., Liu, Y., and Watanabe, Y.: Climate variability patterns and their ecological effects on ecosystems in the Northwestern North Pacific, Front. Mar. Sci., 7, 546882, https://doi.org/10.3389/fmars.2020.546882, 2020.

Manizza, M., Le Quéré, C., Watson, A.J., Buitenhuis, E.T.: Bio-optical feedbacks among phytoplankton, upper ocean physics and sea-ice in a global model. Geophys. Res. Lett. 32, L05603, https://doi.org/10.1029/2004GL020778, 2005.

McWilliams, J. C.: Targeted coastal circulation phenomena in diagnostic analyses and forecast, Dynam. Atmos. Oceans, 49, 3–15, https://doi.org/10.1016/j.dynatmoce.2008.12.004, 2009.

Mellor, G. L. and Yamada, T.: Development of a turbulence closure model for geophysical fluid problems, Rev. Geophys., 20, 851– 875, https://doi.org/10.1029/RG020i004p00851, 1982.

Moon, J.H., Hirose, N., and Yoon, J.-H.: Comparison of wind-tidal contributions to seasonal circulation of the Yellow Sea, J. Geophys. Res., 114, https://doi.org/10.1029/2009JC005314, 2009.

Na, R., Rong, Z., Wang, Z.A., Liang, S., Liu, C., Ringham, M., and Liang, H.: Air-sea CO_2 fluxes and cross-shelf exchange of inorganic carbon in the East China Sea from a coupled physical-biogeochemical model, Sci. Total Environ., 906, 167572, https://doi.org/10.1016/j.scitotenv.2023.167572, 2024.

Najjar, R. and Orr, J. C.: Design of OCMIP-2 simulations of chlorofluorocarbons, the solubility pump and common biogeochemistry, Internal OCMIP Report, LSCE/CEA Saclay, Gif-surYvette, France 1998.

Nishioka, J., Obata, H., Ogawa, H., Ono, K., Yamashita, Y., Lee, K., Takeda, S., and Yasuda, I.: Subpolar marginal seas fuel the Norh Pacific through the intermediate water at the termination of the global ocean circulation, P. Natl. Acad. Sci. USA, 117, 12665–12673, https://doi.org/10.1073/pnas.2000658117, 2020.

Nishioka, J., Obata, H., Hirawake, T., Kondo, Y., Yamashita, Y., Misumi, K., and Yasuda, I.: A review: iron and nutrient supply in the subarctic Pacific and its impact on phytoplankton production, J. Oceanogr., 77, 561-587, https://doi.org/10.1007/s10872-021-00606-5, 2021.

Nitani, H.: Beginning of the Kuroshio, in: Kuroshio: Its Physical Aspects, edited by: Stommel, H. and Yoshida, K., University of Tokyo Press, 129–163, 1972.

Overland, J., Rodionov, S., Minobe, S., and Bond, N.: North Pacific regime shifts: definitions, issues and recent transitions, prog, oceanogr., 77, 92-102, https://doi.org/10.1016/j.pocean.2008.03.016, 2008.

Qui, B.: Kuroshio and Oyashio currents, in: edited by Steele, J. H., Thorpe, S. A., Turekian, K. K., Encyclopedia of Ocean Sciences. Academic, London, 1413-1425, https://doi.org/10.1006/rwos.2001.0350, 2001

Park, J.-Y., Kug, J.-S., Seo, H., and Bader, J.: Impact of bio-physical feedbacks on the tropical climate in coupled and uncoupled GCMs, Clim. Dyn., 43, 1811-1827, https://doi.org/10.1007/s00382-013-2009-0, 2014.

Park, J.-Y., Dunne, J.P., and Stock, C.A.: Ocean chlorophyll as a precursor of ENSO: An Earth system modeling study, Geophys. Res. Lett., 45, 1939-1947, https://doi.org/10.1002/2017GL076077, 2018.

Park, J.-Y., Stock, C.A., Dunne, J.P., Yang, X., and Rosati, A.: Seasonal to multiannual marine ecosystem prediction with a global earth system model. Science, 365, 284-288, DOI: 10.1126/science.aav6634, 2019.

Okamoto, S., Hirawake, T., and Saito, S.: Internal variability in the magnitude and timing of the spring bloom in the Oyashio region, Deep Sea Res. II, 57, 1608-1617, https://doi.org/10.1016/j.dsr2.2010.03.005, 2010.

Reid, P.C., Fischer, A.C., Lewis-Brown, E., Meredith, M.P., Sparrow, M., Andersson, A.J., Antia, A., Bates, N.R., Bathmann, U., Beaugrand, G., Brix, H., Dye, S., Edwards, M., Furevik, T., GangstØ, R., Hátún, H., Hopcroft, R.R., Kendall, M., Kasten, S., Keeling, R., Le Qur, C., Mackenzie, F.T., Malin, G., Mauritzen, C., Olafsson, J., Paull, C., Rignot, E., Shimada, K., Vogt, M., Wallace, C., Wang, Z., and Washington, R.: Chapter 1 Impacts of the Oceans on Climate Change. Academic Press, 56, 1-150, https://doi.org/10.1016/S0065-2881(09)56001-4, 2009.

Séférian, R., Gehlen, M., Bopp, L., Resplandy, L., Orr, J.C., Marti, O., Dunne, J.P., Christian, J.R., Doney, S.C., Ilyina, T., Lindsay, K., Halloran, P.R., Heinze, C., Segschneider, J., Tjiputra, J., Aumont, O., and Romanou, A.: Inconsistent strategies to spin up models in CMIP5: implications for ocean biogeochemical model performance assessment. Geosci. Model Dev. 9, 1827–1851, https://doi.org/10.5194/gmd-9-1827-2016, 2016.

Shchepetkin, A. F. and McWilliams, J. C.: A method for computing horizontal pressure-gradient force in an oceanic model with a nonaligned vertical coordinate, J. Geophys. Res., 108, 3090, https://doi.org/10.1029/2001JC001047, 2003.

Shchepetkin, A. F. and McWilliams, J. C.: The regional oceanic modeling system (ROMS): a split-explicit, free-surface, topography-following-coordinate oceanic model, Ocean Model., 9, 347–404, https://doi.org/10.1016/j.ocemod.2004.08.002, 2005.

Shiozaki, T., Ito, S.-I., Takahashi, K., Saito, H., Nagata, T., and Furuya, K.: Regional variability of factors controlling the onset timing and magnitude of spring algal blooms in the northwestern North Pacific, J. Geophys. Res., 119, 253-265, https://doi. org/10.1002/2013JC009187, 2014.

Siswanto, E., Matsumoto, K., Honda, M. C., Fujiki, T., Sasaoka, K. and Saino, T.: Reappraisal of meridional differences of factors controlling phytoplankton biomass and initial increase preceding seasonal bloom in the northwestern Pacific Ocean. Remote Sensing of Envir., 159, 44-56, https://doi.org/10.1016/j.rse.2014.11.028, 2015.

Son, Y.-T., Chang, K.-I., Yoon, S.-T., Rho, T., Kwak, J.H., Kang, C. K., and Kim, K.-R.: A newly observed physical cause of the onset of the subsurface spring phytoplankton bloom in the southwestern East Sea/Sea of Japan, Biogeosciences, 11, 1319-1329, https://doi.org/10.5194/bg-11-1319-2014, 2014.

Song, Y., and Haidvogel, D.: A semi-implicit ocean circulation model using a generalized topography following coordinate system, J. Comput. Phys., 115, 228-244, https://doi.org/10.1006/jcph.1994.1189, 1994.

Song, Y. T. and Wright, D. G.: A general pressure gradient formulation for ocean models, Part II: Energy, momentum, and bottom torque consistency, Mon. Weather Rev., 126, 3231–3247, https://doi.org/10.1175/1520-0493(1998)126<3231:AGPGFF>2.0.CO;2, 1998.

Sugimoto, S., and Hanawa, K.: Roles of SST anomalies on the wintertime turbulent heat fluxes in the Kuroshio–Oyashio confluence region: influences of warm eddies detached from the Kuroshio extension. J Clim. https://doi.org/10.1175/2011jcli4023.1, 2011.

Taguchi, B., Xie, S.-P., Schneider, N., Nonaka, M., Sasaki, H., and Sasai, Y.: Decadal variability of the Kuroshio Extension: Observations and an eddy-resolving model hindcast, J. Climate, 20, 2357–2377, https://doi.org/10.1175/JCLI4142.1, 2007.

Takahashi, T., Sutherland, S. C., Wanninkhof, R., Sweeney, C., Feely, R. A., Chipman, D. W., Hales, B., Friederich, F., Chavez, F., Sabine, C., Watson, A., Bakker, D. C.E., Schuster, U., Metzl, N., Yoshikawa-Inoue, H., Ishii, M., Midorikawa, T., Nojiri, Y., KÖrtzinger, A., Steinhoff, T., Hoppema, M., Olafsson, J., Arnarson, T. S., Tilbrook, B., Johannessen, T., Olsen, A., Bellerby, R., Wong, C.S., Delille, B., Bates, N.R., and de Baar, H. J.W.: Climatological mean and decadal change in surface ocean pCO2, and net sea-air CO2 flux over the global oceans, Deep-Sea Res. II, 56, 554-577, 2009.

Taniguchi, A.: Differences in the structure of the lower trophic levels of pelagic ecosystems in the eastern and western subarctic Pacific, Prog. in Oceanogra., 43, 289-315, https://doi.org/10.1016/S0079-6611(99)00011-7, 1999.

Taylor, K.E.: Summarizing multiple aspects of model performance in a single diagram, J. Geophys. Res.-Atmos. 106, 7183–7192, https://doi.org/10.1029/2000JD900719, 2001.

Umlauf, L., Burchard, H., and Hutter, K.: Extending the κ-ω turbulence model towards oceanic applications, Ocean Model., 5, 195–218, 5. https://doi.org/10.1357/00222 4003322005087, 2003.

Wang, X., Luo, C., Ge, T., Xu, C., and Xum Y.: Controls on the sources and cycling of dissolved inorganic

https://doi.org/10.5194/egusphere-2024-1509
Preprint. Discussion started: 22 October 2024

carbon in the Chanjiang and Huanghe River estuaries, China: ^{14}C and ^{13}C studies, Limnol. And Oceanogra., 61, 1358-1374, https://doi.org/10.1002/lno.10301, 2016.

Wang, Y., Kang, J., Sun, X., Huang, J., Lin, Y., and Xiang, P.: Spatial patterns of phytoplankton community and biomass along the Kuroshio extension and adjacent water in late spring, Mar. Biol., https://doi.org/10.1007/s00227-021-03846-7, 2021.

Wang, Y., Bi, R., Zhang, J., Gao, J., Takeda, S., Kondo, Y., Chen, F., Jin, G., Sachs, J. P., and Zhao, M.: Phytoplankton distributions in the Kuroshio-Oyashio Region of the Northwest Pacific Ocean: Implications for marine ecology and carbon cycle, Front. Mar. Sci., 9, 865142, https://doi.org/10.3389/fmars.2022.865142, 2022.

Wanninkhof, R.: Relationship between wind speed and gas exchange over the ocean. J. Geophys. Res. 97, 7373–7382m https://doi.org/10.1029/92JC00188, 1992.

Weatherall, P., Marks, K. M., Jakobsson, M., Schmitt, T., Tani, S., Arndt, J. E., Rovere, M., Chayes, D., Ferrini, V., and Wigley, R.: A new digital bathymetric model of the world's oceans, Earth Space Sci., 2, 331–345, https://doi.org/10.1002/2015EA000107, 2015.

Wu, Q., Wang, X., He, Y., and Zheng, J.: The relationship between chlorophyll concentration and ENSO events and possible mechanisms off the Changjiang River estuary, Remote Sens., 15, 2384, https://doi.org/10.3390/rs15092384, 2023.

Yasuda, I.: Hydrographic structure and variability in the Kuroshio–Oyashio transition area, J. Oceanogr., 59, 389–402, https://doi.org/10.1023/A: 1025580313836, 2003.

Yatsu, A., Chiba, S., Yamanaka, Y., Ito, S., Shimizu, Y., and Kaeriyama, M.: Climate forcing and the Kuroshio/Oyashio ecosystem, ICES J. Mar. Sci., 70, 922-933, https://doi.org/10.1093/icesjms/fst084, 2013.

Zhao, H., Dai, M., Gan, J., Zhao, X., Lu, Z., Liang, L., Liu, Z., Su, J., and Cao, Z.: River-dominated pCO_2 dynamics in the northern South China Sea during summer: A modeling study, Prog. Oceanogr., 190, 102457, https://doi.org/10.1016/j.pocean.2020.102457, 2021.

Zhu, K., Chen, X., Mao, K., Hu, D., Hong, S., and Li, Y.: Mixing characteristics of the subarctic front in the Kuroshio-Oyashio confluence region. Oceanologia., 61, 103–113, https://doi.org/10.1016/j.oceano.2018.07.004, 2019.

Zhou, M.J., Shen, Z.L., and Yu, R.C.: Responses of a coastal phytoplankton community to increased nutrients input from the Changjiang (Yangtze) River, Cont. Shelf Res., 28, 1483-1489, https://doi.org/10.1016/j.csr.2007.02.009, 2008.

https://doi.org/10.5194/egusphere-2024-1509
Preprint. Discussion started: 22 October 2024

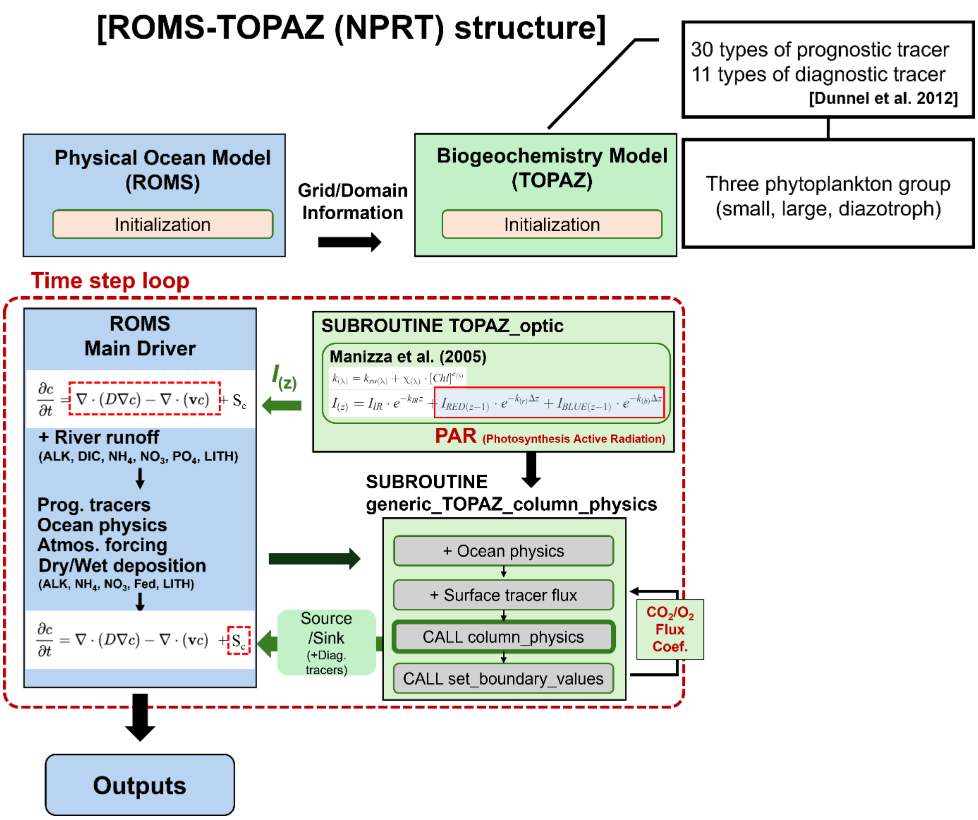

Fig. 1. Flow diagram of the ROMS–TOPAZ model (NPRT). Blue (green) boxes represent the ocean physical (biogeochemical) module. The black arrows indicate the process of transferring oceanic physical information to biogeochemical module, and the green arrows represent vice versa process.

https://doi.org/10.5194/egusphere-2024-1509
Preprint. Discussion started: 22 October 2024

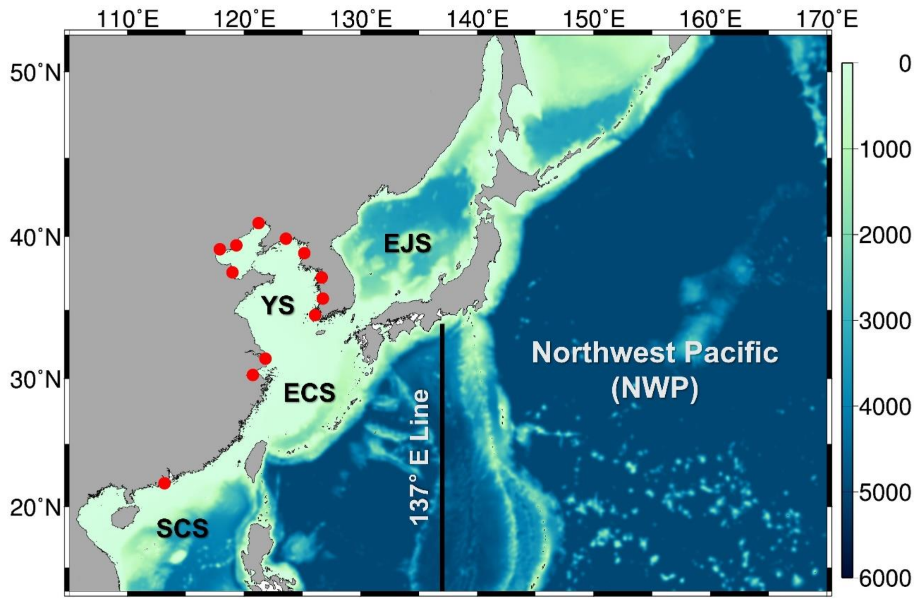

Fig. 2. Model domain and bottom topography for NPRT coupled modeling system. EJS: East/Japan Sea, YS: Yellow Sea, ECS: East China Sea, SCS: South China Sea. The red circles indicate river runoff points, and the black line (137° E line) is the observation line of the Japanese Meteorological Agency (JMA).

https://doi.org/10.5194/egusphere-2024-1509
Preprint. Discussion started: 22 October 2024

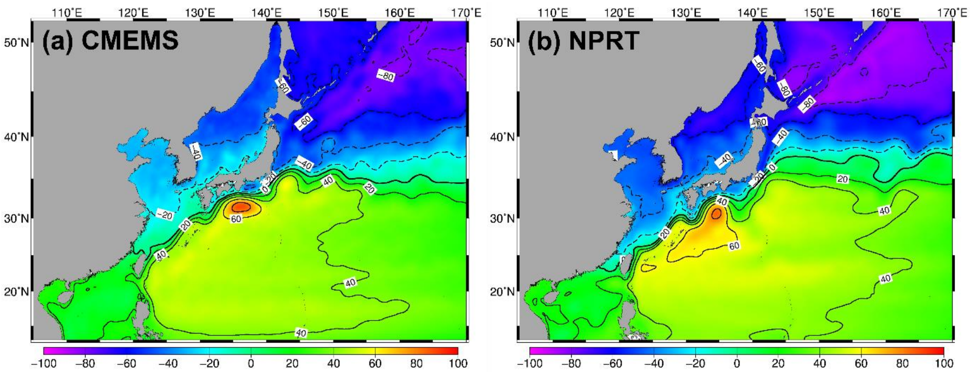

Fig. 3. Distributions of the climatological mean sea surface height (SSH; cm) in (a) satellite altimeters (CMEMS) and (b) NPRT from 2005 to 2014. To compare the two datasets, the spatial mean was subtracted from each one.

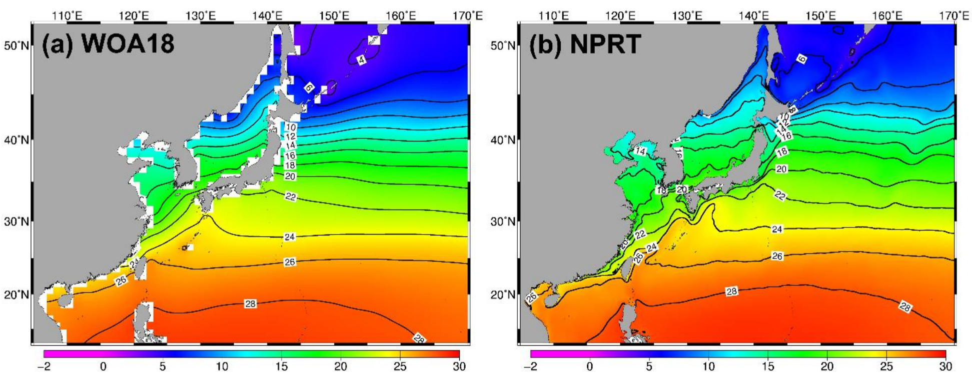

Fig. 4. Same as Fig. 3, except to in the sea surface temperature (SST) from (a) World Ocean Atlas 2018 (WOA18) and (b) NPRT.

https://doi.org/10.5194/egusphere-2024-1509
Preprint. Discussion started: 22 October 2024

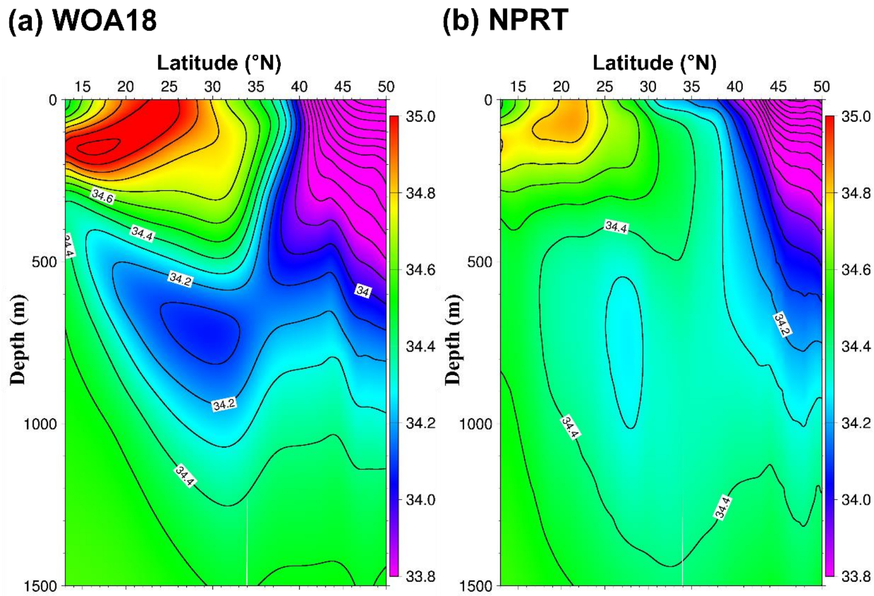

Fig. 5. Vertical structures of the climatological annual-mean salinity in (a) the WOA18 data and (b) NPRT

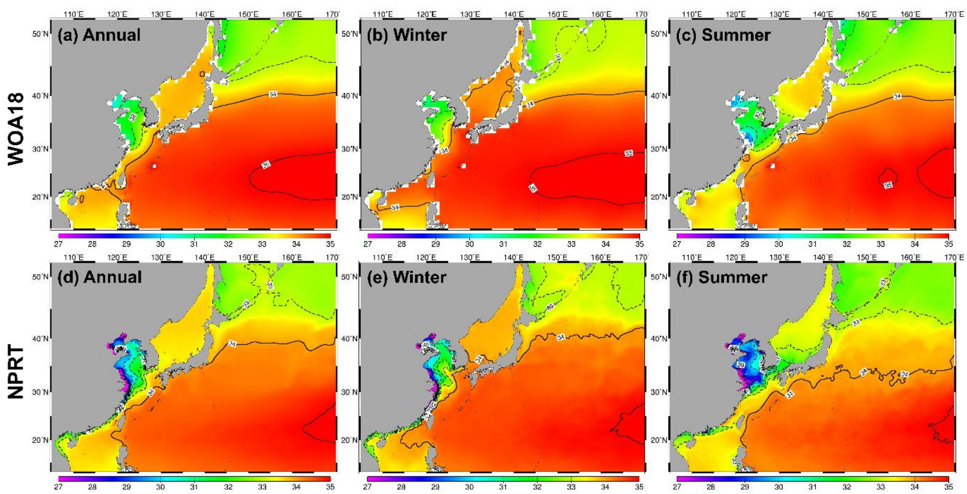

Fig. 6. Distributions of the surface salinity in (a, b, c) the WOA18 data and (d, e, f) NPRT for (a, d) annual mean, (b, e) winter and (c, f) summer.

https://doi.org/10.5194/egusphere-2024-1509
Preprint. Discussion started: 22 October 2024

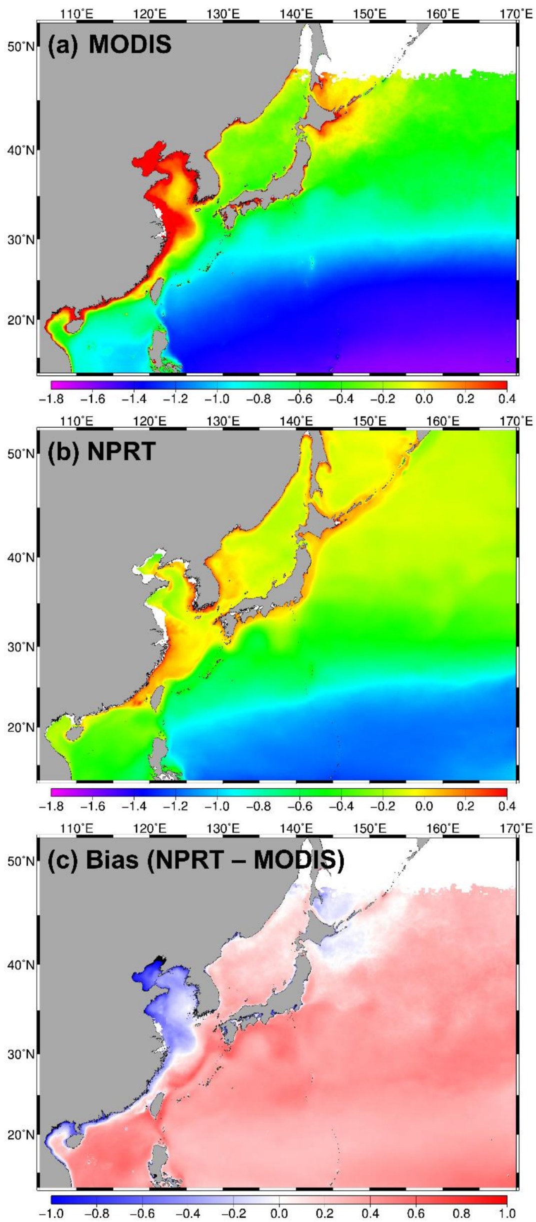

Fig. 7. Logarithm of the climatological annual-mean surface chlorophyll concentrations (μmol kg^{-1}) from (a) MODIS, (b) NPRT, (c) bias of between NPRT and observation (MODIS).

https://doi.org/10.5194/egusphere-2024-1509
Preprint. Discussion started: 22 October 2024

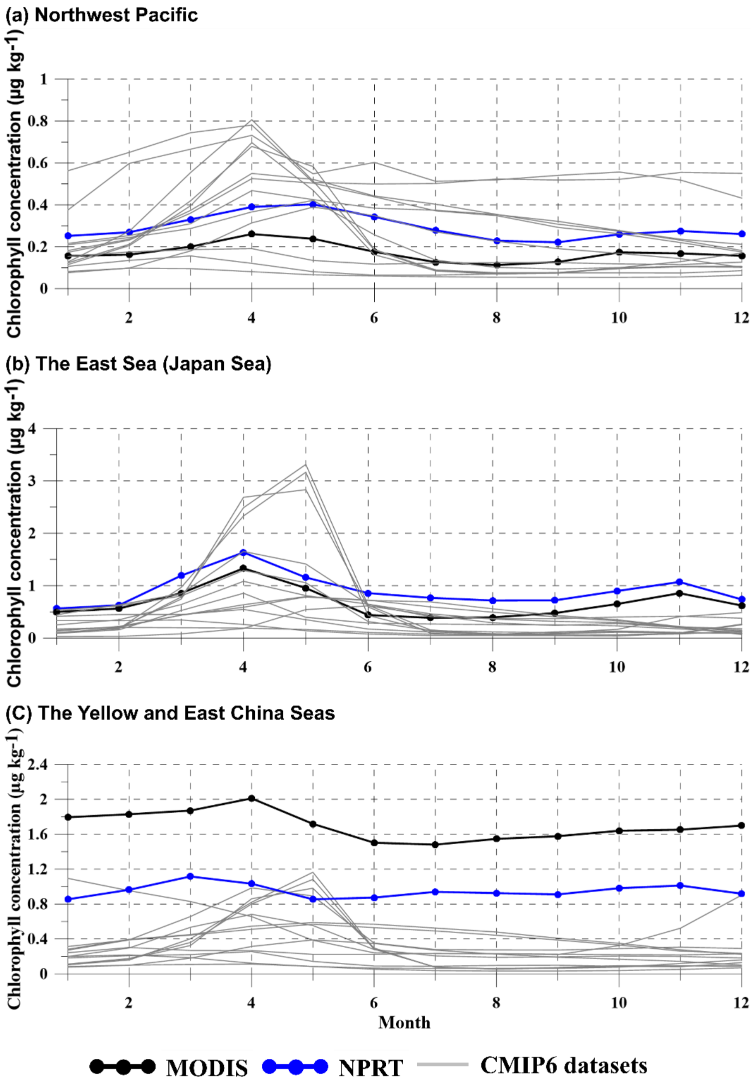

Fig. 8. Seasonal variations of the spatial averaged chlorophyll concentrations (μmol kg^{-1}) in (a) the Northwest Pacific, (b) the East Sea, and (c) the YECS. Black, blue, and light grey lines indicate MODIS, NPRT, and each ensemble model in CMIP6, respectively.

https://doi.org/10.5194/egusphere-2024-1509
Preprint. Discussion started: 22 October 2024

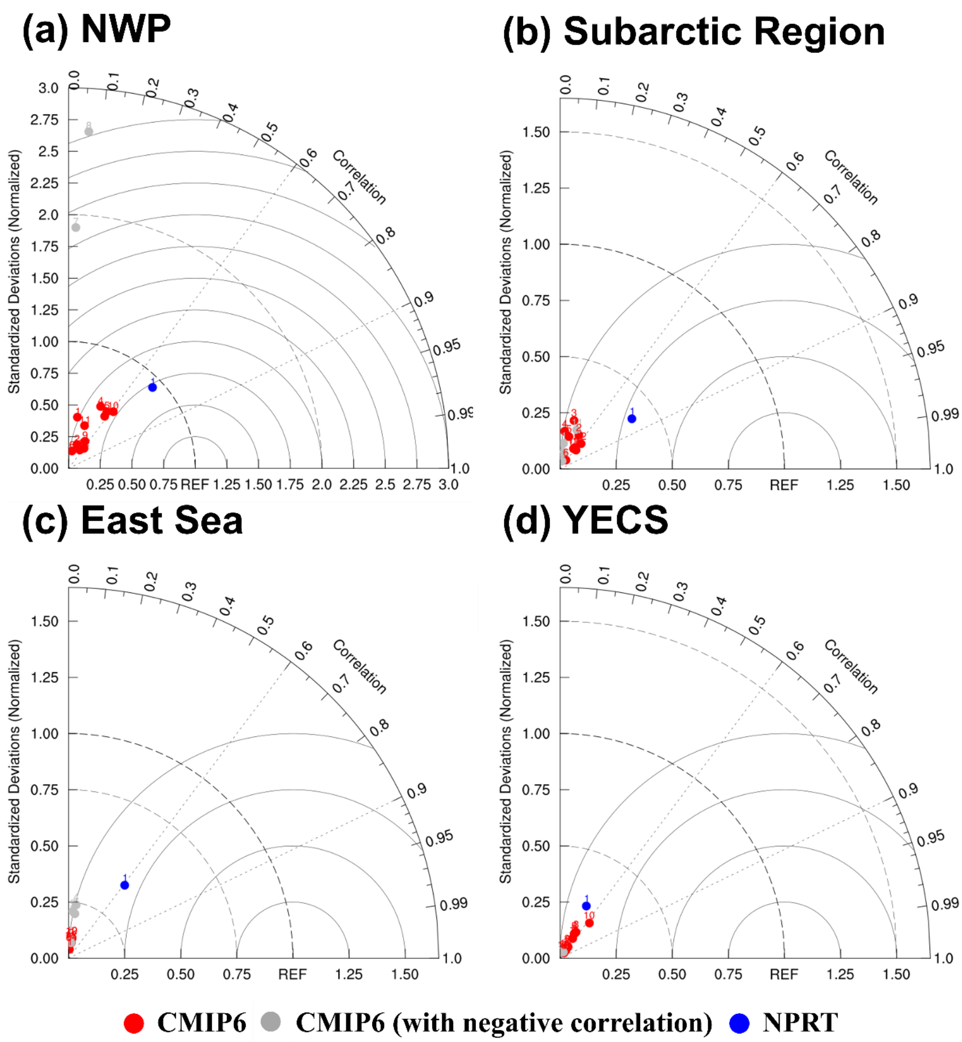

Fig. 9. Taylor diagrams (Taylor, 2001) of spatial two models (NPRT (blue dots) and each ensemble model in CMIP6 (red and grey dots)) for surface chlorophyll concentrations compared to observation (MODIS) at each region. The grey dots in CMIP6 indicate a negative pattern correlation. Taylor diagrams for time were calculated by comparing observational data with annual mean simulated fields of two models (NPRT and each ensemble in CMIP6) in the (a) NWP, (b) subarctic region, (c) East Sea, and (d) YECS, and the numbers represent each ensemble model in Table 1.

https://doi.org/10.5194/egusphere-2024-1509
Preprint. Discussion started: 22 October 2024

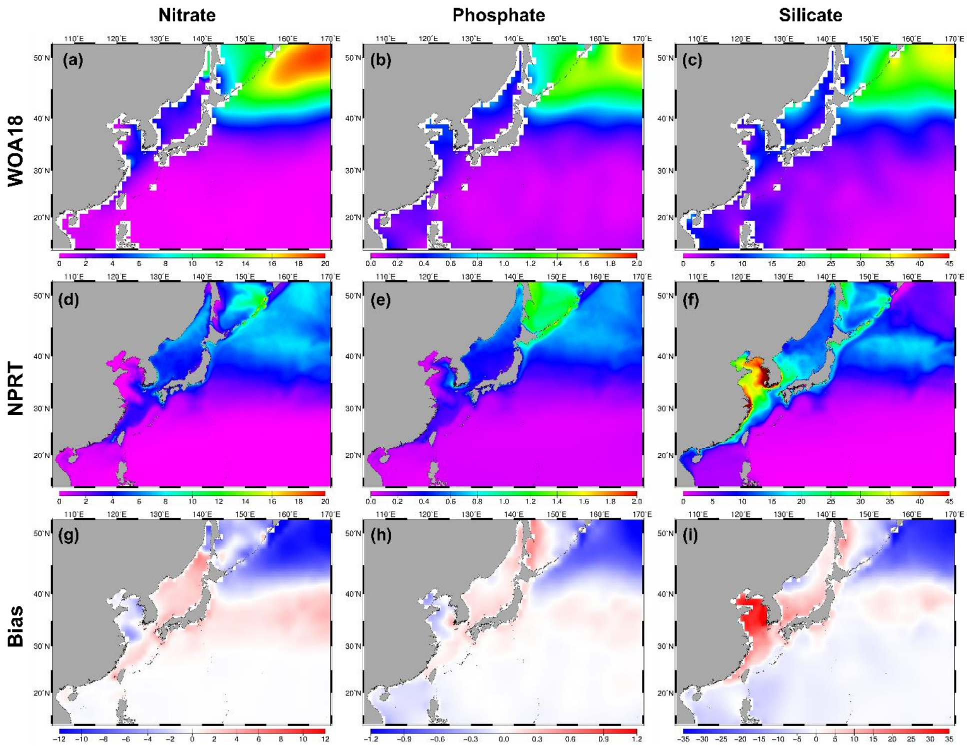

Fig. 10. Horizontal distributions of annual mean surface (a) nitrate, (b) phosphate, and (c) silicate concentrations (μmol kg^{-1}) in the WOA18, and (d, e, f) biases between NPRT and observation (WOA18).

https://doi.org/10.5194/egusphere-2024-1509
Preprint. Discussion started: 22 October 2024

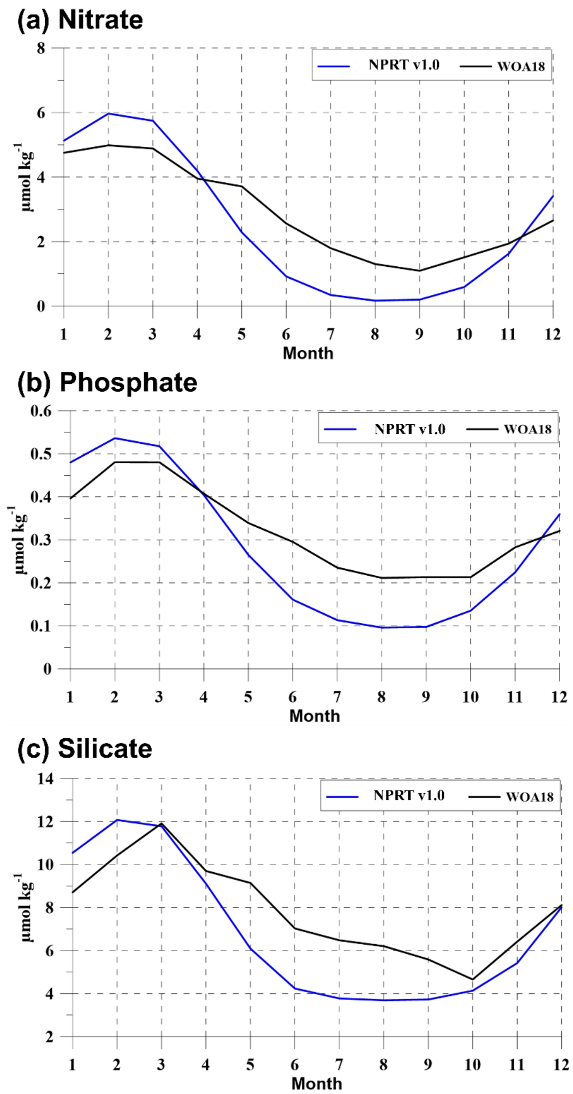

Fig. 11. Seasonal variations of the spatial averaged (a) nitrate, (b) phosphate, and (c) silicate (μmol kg^{-1}) in the Northwest Pacific. Blue and black lines indicate WOA18 and NPRT, respectively.

https://doi.org/10.5194/egusphere-2024-1509
Preprint. Discussion started: 22 October 2024

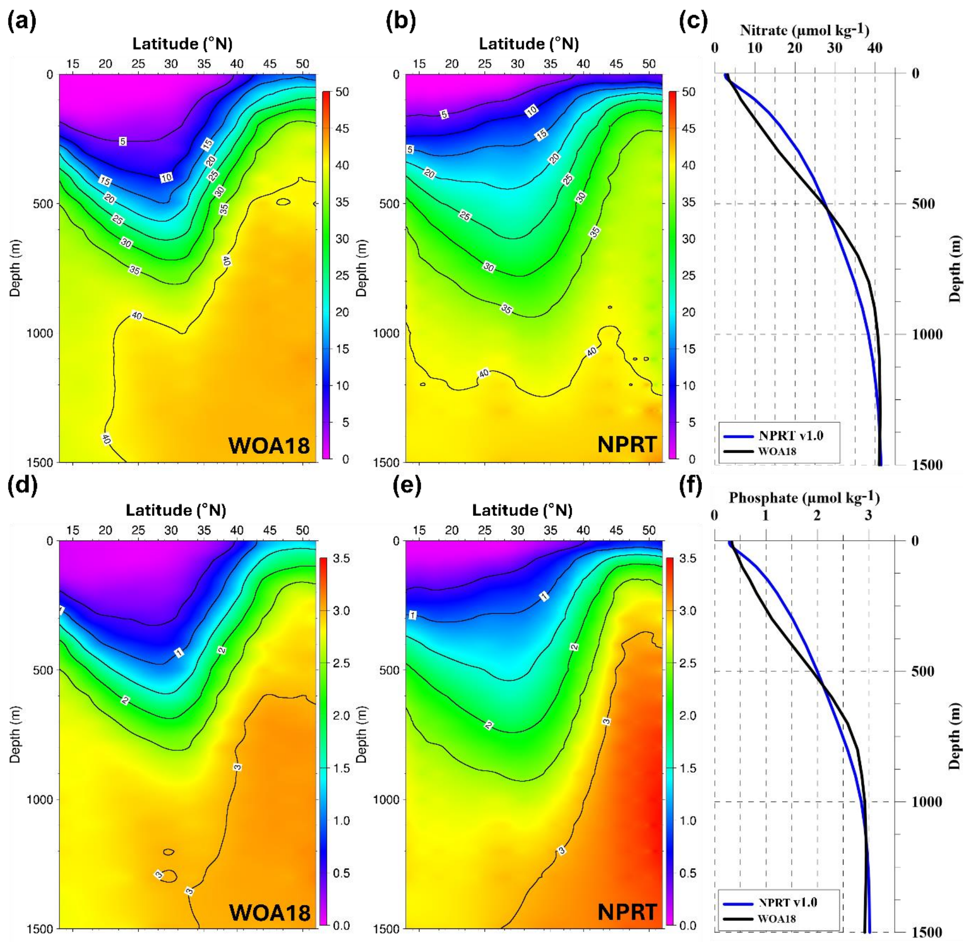

Fig. 12. Vertical structures of the zonal averaged annual mean (a, b, c) nitrate (top) and (d, e, f) phosphate (bottom) concentrations (μmol kg^{-1}) in the Northwest Pacific. (c, f) Blue and black lines indicate WOA18 and NPRT, respectively.

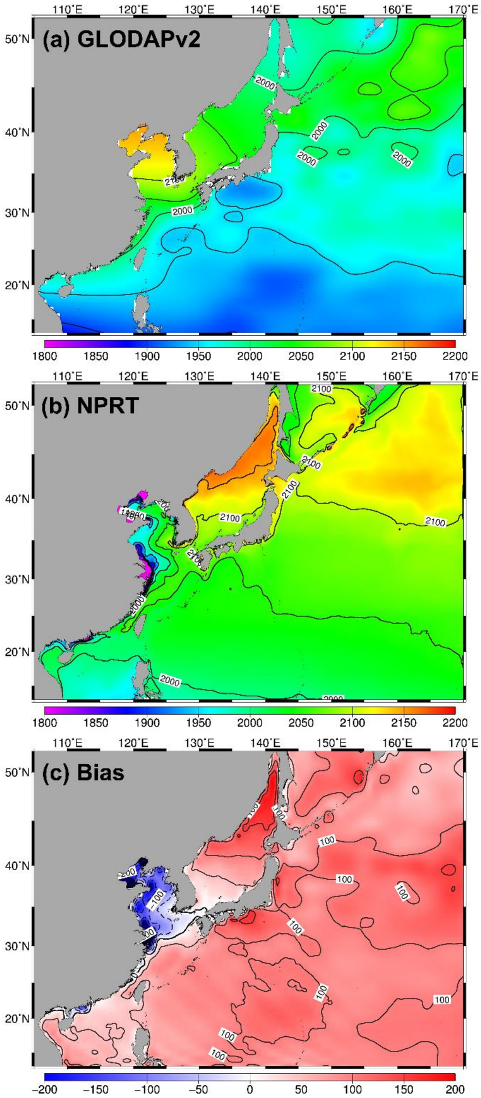

Fig. 13. Horizontal distributions of annual mean surface dissolved inorganic carbon (DIC) concentrations (μmol kg^{-1}) in the (a) GLODAPv2 and (b) NPRT in the Northwest Pacific. Biases (c, f) represent NPRT minus observation (GLODAPv2).

https://doi.org/10.5194/egusphere-2024-1509
Preprint. Discussion started: 22 October 2024

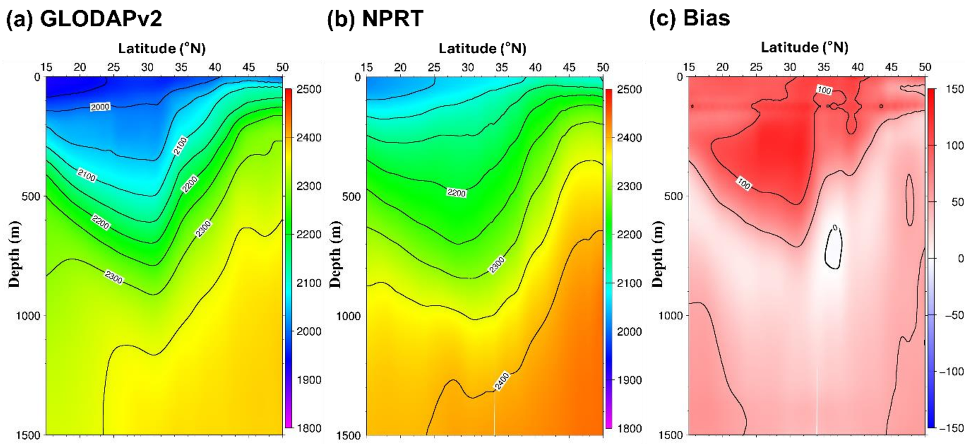

Fig. 14. As in Fig. 13, but the vertical structures of annual mean dissolved inorganic carbon (DIC) concentration (μmol kg^{-1}).

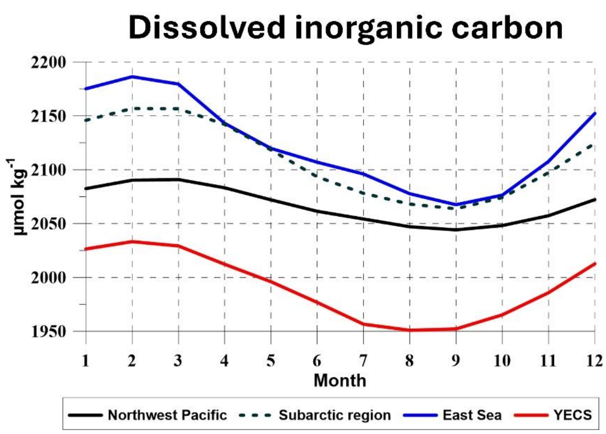

Fig. 15. Seasonal variation of the annual mean surface dissolved inorganic carbon (DIC) concentration (μmol kg^{-1}) in NPRT in the Northwest Pacific (black solid line), subarctic region (north of 40° N in the Northwest Pacific; black dashed line), East Sea (blue line), and the Yellow and East China Seas (YECS; red line).

https://doi.org/10.5194/egusphere-2024-1509
Preprint. Discussion started: 22 October 2024

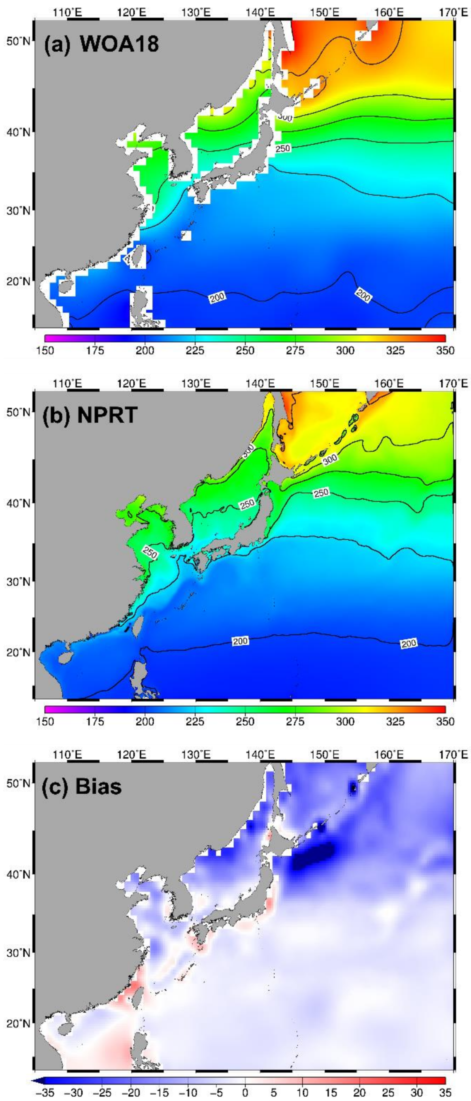

Fig. 16. Horizontal distributions of the annual mean surface dissolved oxygen (DO) concentration (μmol kg^{-1}) in (a) WOA18 and (b) NPRT, and (c) bias between NPRT and WOA18.

https://doi.org/10.5194/egusphere-2024-1509
Preprint. Discussion started: 22 October 2024

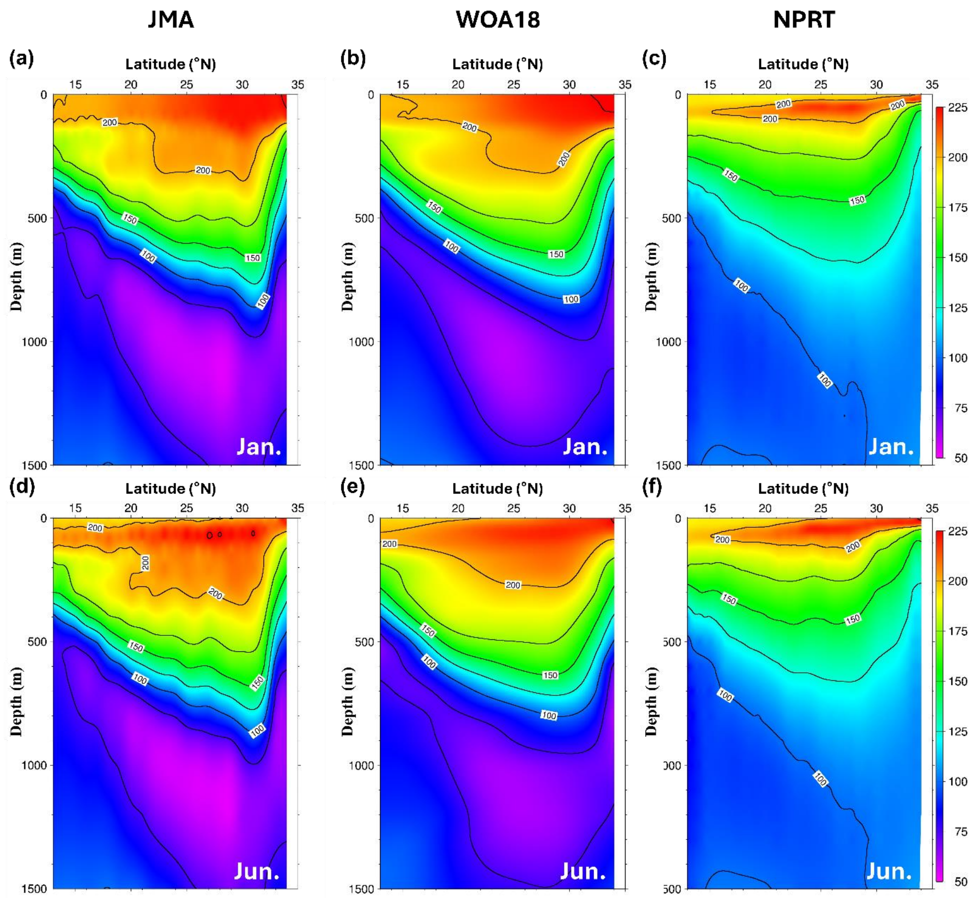

Fig. 17. Vertical structures of the annual mean dissolved oxygen (DO) concentration (μmol kg^{-1}) along 137° E line from (a, d) JMA and (b, e) WOA18, and (c, f) NPRT in January (top) and June (bottom).

https://doi.org/10.5194/egusphere-2024-1509
Preprint. Discussion started: 22 October 2024

Table1. CMIP6 Earth system models were used in this study for comparison with chlorophyll concentration.

Model#	Model name	Model center	Physical/Biochemistry model	Data description
1	ACCESS-ESM1-5	CSIRO	MOM5 / WOMBAT	
2	CanESM5	CCCma	NEMO3.4.1 / CMOC	
3	CESM2	NCAR	POP2 / MARBL	
4	CESM2-WACCM	NCAR	POP2 / MARBL	depth-averaged data
5	CESM2-WACCM-FV2	NCAR	POP2 / MARBL	
6	CMCC-ESM2	CMCC	NEMO3.6 / BFM5.2	
7	MPI-ESM1-2-HR	MPI-M	MPIOM1.63 / HAMOCC6	
8	MPI-ESM1-2-LR	MPI-M	MPIOM1.63 / HAMOCC6	
9	CanESM5-1	CCCma	NEMO3.4.1 / CMOC	
10	EC-Earth3-CC	EC-Earth-Consortium	NEMO3.6 / PISCES v2	
11	MPI-ESM-1-2-HAM	HAMMOZ-Consortium	MPIOM1.63 / HAMOCC6	Surface data
12	NorESM2-LM	NCC	MICOM / HAMOCC	
13	NorESM2-MM	NCC	MICOM / HAMOCC	

https://doi.org/10.5194/egusphere-2024-1509
Preprint. Discussion started: 22 October 2024

Table 2. Summary of the Taylor diagram scores for annual mean surface chlorophyll concentrations in the Northwest Pacific (NWP), subarctic region, East Sea, and the Yellow and East China Sea (YECS) in NPRT and each ensemble model in CMIP6. The subarctic region is north of 40° N in the NWP.

Model	NWP	Subarctic Region	East Sea	YECS
NPRT	1.21	1.64	1.88	2.32
ACCESS-ESM1-5	2.44	3.36	3.07	2.78
CanESM5	2.48	2.71	3.33	2.72
CESM2	1.77	2.47	2.98	2.62
CESM2-WACCM	1.90	2.70	2.96	2.65
CESM2-WACCM-FV2	1.74	2.56	2.92	2.66
CMCC-ESM2	2.72	2.84	3.29	2.79
MPI-ESM1-2-HR	4.32	2.20	3.01	2.58
MPI-ESM1-2-LR	5.77	3.19	2.98	2.73
CanESM5-1	2.13	3.42	3.09	3.50
EC-Earth3-CC	1.60	2.27	2.76	2.27
MPI-ESM-1-2-HAM	2.33	3.29	3.02	3.78
NorESM2-LM	2.22	2.21	2.82	2.60
NorESM2-MM	2.39	2.39	2.81	2.68